

RESEARCH

Open Access



Extracellular matrix protein signaling promotes multi-step cancer vasculogenic mimicry formation

Gabriel Mingo¹, Andrés Valdivia¹, Gema Nicolle Santander^{1,14}, Nicole Babbitt^{1,14}, Varina Aldana¹, Javiera Pradenas¹, Pamela González^{1,14}, Cristóbal Canales^{1,14}, Jorge A. Toledo^{6,7,15}, Carolina Ibáñez^{2,8,9}, Francisco Nualart¹⁰, Manuel Varas-Godoy^{5,11}, Roger Gejman³, Juan Carlos Roa^{3,9,14}, Andrea Ravasio⁴, Cristina Bertocchi^{1,12} and Gareth I. Owen^{1,2,9,13,14*}

Abstract

Cancer vasculogenic mimicry (VM) is the formation of vasculature structures in the absence of endothelial cells. We previously established an in vitro model that facilitates the formation of a lumen-containing and fluid-conducting tubular structures after 4 days of cancer cell growth on Matrigel. Herein, we mechanistically characterize this model in breast and ovarian cancer cell lines demonstrating distinct phases of VM formation and the dependence of specific extracellular matrix proteins. We report that VM occurs in four distinct stages. Firstly, alignment, migration then clustering delineate the area of the future tubular structure. Secondly, contraction of aligned structures followed by loss of attachment of some cells and cellular blebbing. Thirdly, a phase of mass proliferation followed by the raising of specific areas of the cancer cell mass above the Matrigel (bridge). Finally, the formation of a cell monolayer closes the tubular structure, forms a glycoprotein-rich luminal lining, then elevates the structure. Only later stages of VM require AKT and FAK signaling, as confirmed by chemical inhibition and phosphorylation analysis. We demonstrate that the lining of the tubular lumen is rich in laminin. Furthermore, the presence of Laminin 111 (but not collagen I) is sufficient in the extracellular matrix (Matrigel) for VM to occur and we confirm that integrin $\beta 1$, but not integrin $\beta 3$, is required and this protein changes location during the formation process. RNASeq analysis suggests that VM formation principally occurs through post-transcriptional regulation. As VM is associated with poor patient survival VM, an understanding of the mechanism of VM may bring to light novel biomarkers and anticancer targets.

Keywords Vasculogenic mimicry, Ovarian cancer, Breast cancer, Extracellular matrix, Integrins

*Correspondence:
Gareth I. Owen
gowen@bio.puc.cl

Full list of author information is available at the end of the article



© The Author(s) 2025. **Open Access** This article is licensed under a Creative Commons Attribution-NonCommercial-NoDerivatives 4.0 International License, which permits any non-commercial use, sharing, distribution and reproduction in any medium or format, as long as you give appropriate credit to the original author(s) and the source, provide a link to the Creative Commons licence, and indicate if you modified the licensed material. You do not have permission under this licence to share adapted material derived from this article or parts of it. The images or other third party material in this article are included in the article's Creative Commons licence, unless indicated otherwise in a credit line to the material. If material is not included in the article's Creative Commons licence and your intended use is not permitted by statutory regulation or exceeds the permitted use, you will need to obtain permission directly from the copyright holder. To view a copy of this licence, visit <http://creativecommons.org/licenses/by-nc-nd/4.0/>.

Introduction

One of the hallmarks of cancer is the process of angiogenesis, which is the formation of new blood vessels from the existing circulation [1]. However, nature has derived other methods to facilitate blood transport in the body. In physiology, macrophages have been shown to rearrange to form tubular structures that allow transport [2]. The growing trophoblast can form so-called spiral arteries present at the maternal fetal interface [3, 4]. Interestingly, before the evolution of endothelial cells, some invertebrates and cephalochordates (e.g. *Amphioxus*) possessed a circulatory system that was not lined by cells, but by a glycoprotein rich layer [5].

In pathophysiology, namely cancer, another type of irrigation has been identified. Cancer Vasculogenic Mimicry (VM) is the formation of vessel-like structures uniquely from cancer cells [6]. Tubular structures inside the tumor are speculated to connect to the blood supply to enhance oxygen and nutrient supply, and potentially allow an easier means for metastasis [7]. VM can be observed *in vivo* in histological samples with a double stain with Periodic Acid Schiff (PAS), a glycoprotein marker, together with the absence of endothelial markers such as CD31 or CD34 [8]. VM was first discovered in 1999 by Maniotis in a uveal melanoma, and has since been observed in the majority of known cancers, associating with extremely poor patient survival [6]. To date there has been no evidence that suggests that VM associates with cancer stage, grade, tumor size or patient age [9, 10].

While consensus is present on the identification of VM *in vivo* (although a better marker than the absence of CD31 or CD34 is required), there is still controversy over an *in vitro* model for VM. The vast majority of cancer cells typically form a monolayer on cell-culture treated plastic or glass but tend to form projections and intercellular connections on a 3D matrix. Numerous publications have reported the interconnection of cancer cells on an extracellular matrix (ECM, Matrigel or similar hydrogel matrix), however many publications do not show the presence of a lumen or the ability to contain and compartmentalize fluid. Building upon the foundation of other laboratories, our laboratory proposed a model of VM *in vitro* that demonstrated the formation of a glycoprotein-rich lumen that was capable of fluid conduction [11–14]. Moreover, this tubular structure presented diameters of 50 to 200 microns and included numerous cancer cells [9]. In accordance with other authors, we reported that the PI3K pathway was essential for complete tubular formation and that classic anti-angiogenics did not inhibit the process [9, 10, 14].

The ECM that forms the interstitial matrix and the basement membrane is principally composed of collagen, laminin and fibronectin, together with other glycoproteins, polyglycans and enzymes, which have different

proportions, characteristics, and functions depending on the tissue function and location in the body [15, 16]. It is unknown if ECM proteins are required to activate the VM process or merely to provide the opportunity for structures to form in 3D. Matrigel, the most widely used substitute for the ECM *in vitro*, is also rich in these components, however the principal laminin present is 111, not laminins 411 and 511 which are main laminin isoforms found in endothelial and perivascular basement membranes [17, 18]. Laminin in the ECM directly communicates to the cell using a plethora of transmembrane proteins of which three major classes have been reported: $\beta 1$ and $\beta 3$ integrins, dystrophin glycoprotein complex and Lutheran blood group glycoprotein [17].

ECM ligand recognition by integrins leads to a conformational change of integrin, with an extension of the heterodimer that eventually transforms into a force-transducer. This change of conformation allows the cytoplasmic tail to initiate the assembly of focal adhesion proteins to structurally and functionally link ECM ligands to the cytoskeleton and lead to downstream signal transduction [19]. Among numerous signaling pathways, integrins are known to activate the FAK/PI3K pathway [20]. Integrin-ECM binding leads to recruitment, autophosphorylation and activation of the Focal Adhesion Kinase (FAK). This creates an available binding site for PI3K, its phosphorylation and activation [20]. From this point, PI3K can activate many signaling pathways, of which the AKT pathway is reported to promote cellular proliferation and migration [21]. This pathway is described previously in VM formation and is independently associated with a poor patient prognosis [21]. Proliferation and migration in an ECM/Matrigel requires the remodeling of the matrix, and in accordance metalloproteases are influential in VM formation [7, 11].

Building upon the aforementioned studies, the objective of this article is to decipher the triggers required, the role of the ECM, the signaling pathways involved, and general mechanism of the formation of VM in reproducible *in vitro* models of breast and ovarian cancer. The nature and structure of the tubular structure is also examined.

Materials and methodology

Reagents

Cell culture reagents including were used as previously described [9]. Growth factor reduced, phenol red-free Matrigel (356231, here after called Matrigel) was purchased from Corning (Bedford, MA). 3-D Culture Matrix Rat Collagen I (3447-020-01) and 3-D Culture Matrix Laminin I (3446-005-01) were purchased from R&D Systems (Minneapolis, MN). siRNA against Integrin $\beta 1$ (sc-35674), primary antibodies Integrin $\beta 1$ (P5D2, sc-13590), Cortactin (H-5, sc-55579) and Integrin $\beta 3$

(2C9.G2, sc-46655) were purchased from Santa Cruz Biotechnology (Dallas, TX). Primary antibody beta-actin and pan-Laminin (ab-1, RB082A1) were purchased from Invitrogen (Waltham, MA). Secondary antibodies goat anti-mouse IgG HRP, goat anti-mouse IgG cross-adsorbed Alexa Fluor 555 and goat anti-rabbit IgG cross adsorbed Alexa Fluor 555 were purchased from Invitrogen (Waltham, MA). Secondary antibody goat anti-rabbit IgG-HRP conjugate was purchased from Bio-Rad (Hercules, CA). Phalloidin Alexa Fluor 488 was purchased from Invitrogen (Waltham, MA). LY-294,002 hydrochloride (iPI3K), PF-573,228 (iFAK) and AKT inhibitor IV (iAKT) (all Merck Sigma-Aldridge, Germany) have been previously demonstrated to have specific action in ovarian cancer lines at concentrations used herein [22–24].

Cell lines & primary cultures

HEY-A8 and MDA-MB-231 were obtained from ATCC (Manassas, VA) [25, 26]. GFP-HEY-A8 (GFP) cells were generated as described [27, 28]. All cells were routinely passaged in DMEM-F12 10% FBS and 1% penicillin/streptomycin and continually assessed for mycoplasma. Primary ovarian cancer cultures derived from ascites were obtained as described [29–31].

Patient samples

Human ovarian cancer ascites samples were obtained from the Hospital Pontifical Catholic University of Chile with prior written informed consent. All experiments were performed in accordance with the Declaration of Helsinki and the research protocol was approved by the Ethics Committee of the Pontifical Catholic University of Chile, Protocol ID 210,622,007 and approval resolution No. 012793 (19/4/22).

Inclusion criteria

Female subjects over 18 years of age within no ethnic exclusion having confirmed stage III or IV ovarian cancer from the RedUC-Christus hospital in Santiago, Chile.

SiRNA transfection

Transfected was performed using Lipofectamine 2000 (11668019, Invitrogen, Waltham, MA) using manufacturer's protocol on 3 cm cell culture plates. Cells were between 60 and 80% confluent at transfection. Cell culture medium was replaced with 2 mL of Opti-MEM I reduced serum medium (31985062, Gibco Life Technologies, Waltham, MA) one hour prior to the transfection. 5 mL of Lipofectamine 2000 was diluted in 250 mL of Opti-MEM I reduced serum medium and incubated for 5 min. In parallel, 100 pmol of siRNA was diluted in 250 mL of Opti-MEM medium. After 5 min the siRNA dilution with the Lipofectamine 2000 dilution was mixed 1:1 and incubated for 20 min at room temperature. 500 mL

of the siRNA-lipid complex was added to the cells and incubated for 6 h. Cells were maintained in DMEM-F12 10% FBS and 1% penicillin/streptomycin.

VM in vitro assay: three dimensional (3D) cultures

Experiments were performed as previously established by our group [9]. In brief, 18 × 18 mm glass coverslips (0101030, Marienfeld, Lauda-Königshofen, Germany) were ethanol-washed, air-dried and placed in pre-chilled 6-well culture plates (140675, Thermo Scientific, Waltham, MA). Each. Coverslip was coated with 250 μL cold Matrigel and incubated at 37 °C for 45–60 min to allow the Matrigel to Gel. Cells were trypsinized, counted and resuspended in 200 μL of culture medium (RPMI-1640, 15% FBS and 1% penicillin/streptomycin) before seeding onto Gellified Matrigel-coated coverslips. Cells were incubated at 37°C for 1 h to allow adhesion to the matrix before supplementation with 3 mL of culture medium. Culture medium was changed every 2 days. Denatured Matrigel was created by heating Matrigel to 65°C for 10 min, to denature any proteins present in the matrix. Cells grow to a monolayer on this matrix but do not form VM structures. For experiments with chemical inhibitors the culture medium was changed daily.

RNA extraction and RNA sequencing

From VM assay, cells were extracted in TRIzol reagent (15596018, Invitrogen, Waltham, MA). The cell solution (700ul) was incubated for 5 min at room temperature and 150 mL of chloroform (102444, Merck, Darmstadt, Germany) added before agitation for 15 s. A further incubation of 3 min occurred before centrifugation at 12,000 G for 15 min at 4 °C. The aqueous phase was transferred to a new microcentrifuge tube and 380 mL of isopropanol (109634, Merck, Darmstadt, Germany) added before an incubation of 10 min at room temperature. After centrifugation at 12,000 G for 10 min at 4 °C the pellet was three times with 700 mL of 75% ethanol (samples air dry for 5 min during washing). Samples were resuspended in 20 μL of DEPC water (AM9915G, Thermo Fisher) and incubated for 10 min at 55 °C. The RNA samples were sent to BGI Genomics in Hong Kong, to be sequenced. Samples were sequenced using the DNBseq platform and the bioinformatics were performed by BGI Genomics. The RNA data is available on: <https://www.ncbi.nlm.nih.gov/geo/query/acc.cgi?acc=GSE263232>.

Conventional PCR

RNA samples were converted into cDNA as reported previously [32]. SMIM11A forward primer (5'-GGACG GTAGAACGTCGTGGTT-3'), SMIM11A reverse primer (5'-GACCAACACCGTAGGCTTGA-3'), beta actin forward primer (5' GCAAAGTCCTGTACGCCAAC-3'), beta actin reverse primer (5'-ACATCTGCTGGAAGGT

GG-3') using the following protocol: 5 min at 95 °C; 45 s at 95 °C, 30 s at 55 °C, 60 s at 72 °C for 35 cycles; and 5 min at 72 °C.

MTS viability assay

The MTS (3-(4,5-dimethylthiazol-2-yl)-5-(3-carboxymethoxyphenyl)-2-(4-sulfophenyl)-2 H-tetrazolium) assay was performed as previously described by our laboratory [33]. Each point was performed in 5 experimental replicates, in three biological experiments ($n=3$).

Protein extraction and Western blot

Protein extraction and Western blotting were performed as previously described [34, 35]. Protein quantification was performed using the Pierce BCA Protein Assay Kit (23225, Thermo Scientific, Waltham, MA). 30 µg of total protein lysates were used for each sample. Blots were developed using SuperSignal West Pico PLUS Chemiluminescent Substrate (34580, Thermo Scientific, Waltham, MA).

Phosphoarray analysis

From VM assay, protein lysate was extracted as previously described [34, 35]. The protein was derived from HEY-A8 cancer cells growing either on denatured Matrigel (not forming VM, methodology described above) or growing on Matrigel (forming VM). Protein lysates (400 µg at a concentration of 2 µg/µL) were sent to Full Moon BioSystems (CA, USA) to be analyzed by the Phospho Explorer Antibody Array. The bioinformatic analysis of the microarray was performed by *Fullmoon Biosystems* (CA, USA) and is specified in more detail on their website: <https://www.fullmoonbio.com>. Briefly, for each spot on the array, median signal intensity is extracted from array image. An average signal intensity of replicate spots was generated from the mean value of median signal intensity of replicate spots for each antibody. Normalized data is achieved from the average signal intensity of replicate spots divided by the median signal. Data is normalized to the median value of average signal intensity for all antibodies on the array. Finally, fold change between control (not forming VM) and treatment samples (protein from cells forming VM) from normalized data are calculated as treatment sample divided by control sample. Fold change values ≤ 0.5 and ≥ 2 were considered as significant changes.

Immunofluorescence and confocal imaging

Culture medium was extracted from VM assays and 2 mL of 4% PFA was added. Cells were washed with 1X PBS twice for 3 min. NH₄Cl 50 mM was added to the cells for 10 min and washed with 1X PBS twice for 3 min. Permeabilization with 0.1% PBS-Triton for 5 min was followed by washing with 1X PBS twice for 3 min. The samples

were blocked with PBS-BSA 2% for 30 min and primary antibodies were added at a dilution of 1:50 (integrin β1) or 1:100 (cortactin) for 1 h at room temperature in a dark wet chamber. Cells were washed 3 times with 1X PBS for 3 min and secondary antibodies added at a dilution of 1:1,000 with 1X phalloidin for 1 h at room temperature in a dark wet chamber. Samples were washed with 1X PBS 3 times for 3 min and DAPI was added at a dilution of 1:75,000 for 30 s. Cells were washed with dH₂O for 5 min and then mounted onto a microscope slide with 10 µL of Fluoromount G (17984-25, Electron Microscopy Science, Hatfield, PA). Slides were air-dried overnight at room temperature in the dark. HEY-A8 images were acquired using a Nikon Ti-2 inverted confocal microscope (Nikon Instruments Inc, Melville, NY) and an ISM 880 ZEISS with Airyscan detection (Leica Microsystems, Wetzlar, Germany), and analyzed using either the NIS-Elements Viewer 5.21.00 or Zen 2.3 black, respectively. MDA-MB-231 images were acquired using a Leica Zeiss LSM 780 confocal microscope (Leica Microsystems, Wetzlar, Germany) and analyzed by software Zen 3.8 Lite. For quantification of integrin β1 intensity on the plasmatic membrane, specific masks were created and the fluorescent average intensity was calculated for each experimental unit. For quantification of cortactin to nuclei (DAPI) ratio in the upper and lower layers of the tubular structures, pixel values were gathered for each image in the z-stack between 0 and 10 µm from Matrigel or the upper layer between 30 and 40 µm.

Statistical analysis

Results are shown as mean \pm SEM from at least three independent experiments. Either Student's t-test or one-way ANOVA were used followed by post hoc adjustment. For fluorescence quantification the values were compared between conditions (control vs. VM) with Welch's t test. For the comparison between formation times of VM, ANOVA was used followed by post hoc adjustment. Analysis was performed with GraphPad 9.4.1 (San Diego, CA). P value of <0.05 was considered statistically significant.

Results

Stages of VM formation

In our previous studies we reported that cancer cells are capable of forming tubular structures on Matrigel after 4 days in culture [9]. Based on staining with PAS, we reported that the lumen-containing vessel was lined with a glycoprotein rich coating with the cancer cells on the outside closing this structure. To provide a mechanistic explanation of the process we examined in detail both the timing and nature of the tubular formation and the constituents of the glycoprotein-rich lining.

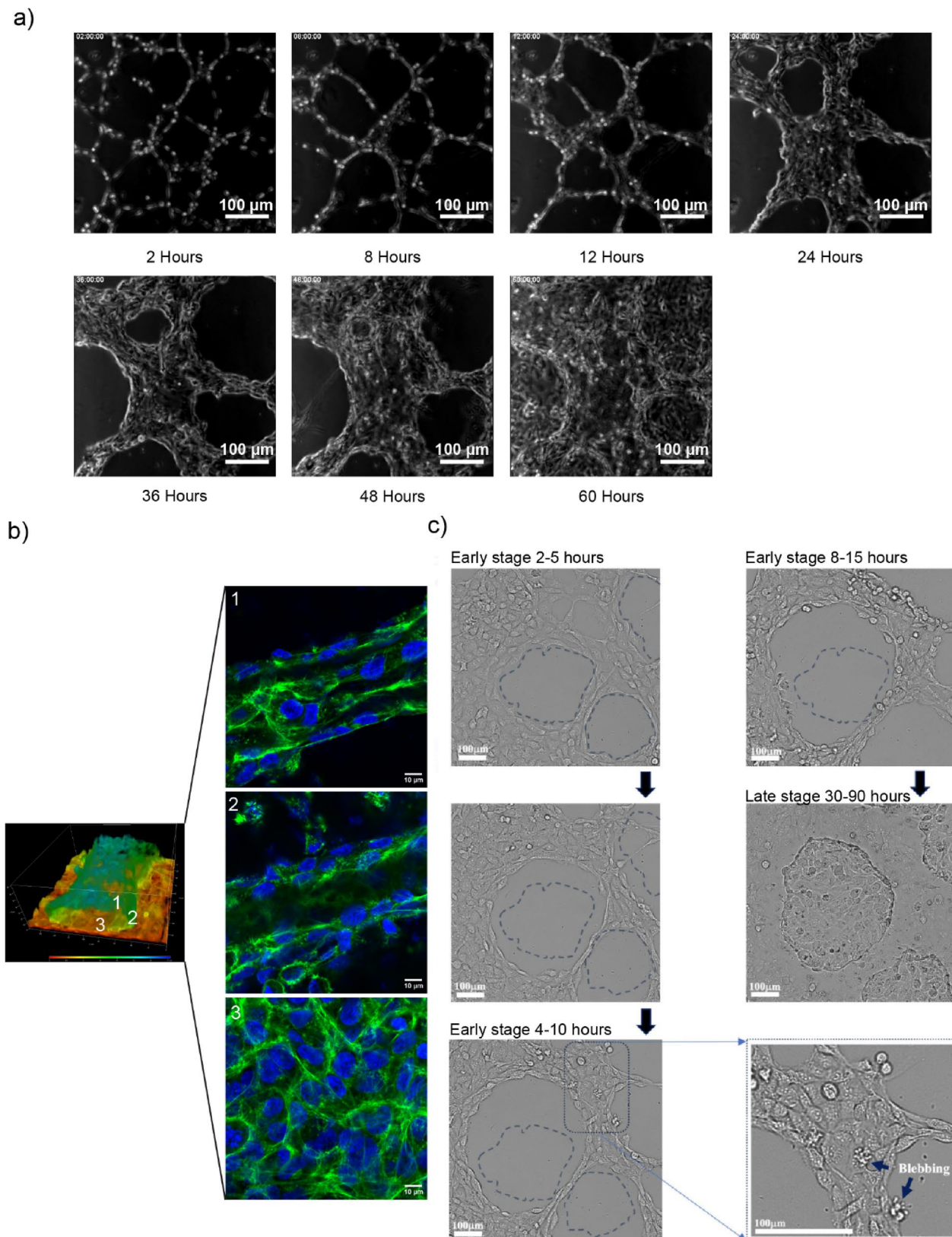


Fig. 1 (See legend on next page.)

(See figure on previous page.)

Fig. 1 Time lapse photography and structure of VM formation in the HEY-A8 cancer cell line **A** HEY-A8 cells were seeded onto Matrigel and placed in a temperature-controlled microenvironment for observation by time-lapse light microscopy. Timepoints of from 2 up to 60 h are shown. **B** 3D reconstruction of the tubular structure. Images were taken by immunofluorescence. F-actin (phalloidin) and the cell nucleus stained by DAPI (blue). In (1) there is the highest part of the structure. In (2) is a cross-section of the middle of the tube the walls as a lumen can be observed. In (3) the base of the structure, composed of a monolayer of cells. **C** Contraction and blebbing are present in the formation of VM. Time lapse MuviCyte Live Imaging System time-lapse (Perkin Elmer) microscopy stills of VM formation in the HEY-A8 cancer cell line between during the course of VM formation ($N=3$ timelapse, representative images from one experiment). Segmented lines depict the original location at the 2–5 h time point before contraction. The lower right panel represents is a magnification of the forming structure to show the presence of rounded cells and blebbing

In supplementary video 1 and in Fig. 1 we demonstrate that tubular formation *in vitro* occurs in four distinct steps which starts with individual cells aligning to form linear aggregates that, upon cell proliferation, eventually form a tubular structure that is elevated in the culture plate by a monolayer than forms below. When observed after 4 days (Fig. 1B), confocal microscopy shows the presence of an elevated structure containing a hollow lumen. From z-stack reconstruction we observe that the base of the lumen-containing structure is consistent with the cell monolayer, then moving further up we observe only the walls of the structure, until finally cells close the top of the tubular structure. Although we originally reported that this process requires 4 days, we now report that in certain areas of the culture plate this process can occur faster, sometimes in less than 60 h. This can be clearly observed by comparing the formation time between supplementary video 1 and 2, and thus for the purposes of this characterization, we have stated a range of times in which each step in the process could occur. The first step (alignment and migration) occurs between 0 and 2 h after plating the cancer cells migrate to align on Matrigel and form cellular connections. This process is then accompanied by extensive cell migration (please refer to supplementary video 1 and 2) where cancer cells migrate along linear cell aggregates. Cellular proliferation occurs at this step. As mentioned previously, many cancer cells (and non-cancerous cells) behave in a similar way when seeded on Matrigel, however it is advancement to the following steps that define VM.

The second step (contraction, blebbing, proliferation and bridge formation) is shown in Fig. 1C (and best observed in supplementary video 2) and involves contraction of the mass of cells. This contraction occurs over a few hours and reduces drastically the area of the plate covered by cells. Once this contraction finishes, certain cells appear to reorientate in the forming structure and circularize. This minority of cells undergoes what appears to be extensive blebbing (final panel in Fig. 1C and supplementary video 2). The consequence for this potential blebbing is currently unknown, however these cells either undergo apoptosis or proliferation then reincorporate into the tubular structure. Experiments are currently ongoing to understand the role of blebbing. This second phase, which commences around 6 h and continues until approximately 32 h, is also a phase of massive

proliferation with formation of a multilayered aggregate and the final location of the tubular structure is defined (Figs. 1C and 8–15 h). Whether directly due to the contractile process or not, bridges now appear where cells detach from the Matrigel and move upwards as observed in the 8- and 24-hour time points on Fig. 2. This bridge structure is shown in greater detail in Supplementary Fig. 1. The third stage is tube closure, when cells at the edge of the tubular structure spread to form a monolayer across the plate. Confocal microscopy at each time point shows that these cells close the tubular structure from below as shown in panel B in Fig. 2. This can be seen by comparing 48 h with 96 h in Fig. 1 (and the formation of a monolayer below the structures in supplementary video 1). Interestingly, the formation of the monolayer cells can be seen at 9 h on supplementary video 2 (this is exceptionally fast, it usually takes at least 24 h longer). The final stage (Stage 4, elevation, and luminal lining formation) occurs when these tubular structures are elevated above the cell monolayer and formation of a glycoprotein-rich luminal lining can be seen. This can be observed in supplementary video 1, as the newly formed monolayer is now in focus and the tubular structure that formed first is elevated and out of focus. Interestingly, cortactin immunoreaction was repeatedly stronger in the cells in the upper region of the structure, despite actin (phalloidin) and nuclei (DAPI) in cancer cells were notably present below (panel 96 h, Fig. 2). We quantified these levels in the upper and lower regions of the tubular structure and found a statistical difference when normalizing to abundance of cell nuclei (please refer to supplementary Fig. 2). From 60 h, confocal microscopy of the tubular structure reveals the presence of a glycoprotein-lined luminal structure. Figure 2C presents a schematic representation of this four-step process.

Laminin is present in the matrix of VM lumen

While we previously identified a glycoprotein-rich inner lining of the completed tubular structure, we can now demonstrate that a major luminal component is laminin. Immunoreaction of a pan-laminin antibody was observed in tubes formed from HEY-A8 and MDA-MB-231 cells (Fig. 3A and D, respectively). Using an orthogonal view, laminin is present principally within the interior of the tube (Fig. 3B-E). Although laminin is uniformly distributed in the glycoprotein matrix on the luminal side of

the tube, it is not the only protein. Using picrosirius red staining, which is used to observe collagen I and collagen III fibers, it could be seen that collagens I or III were present on the glycoprotein matrix, but they weren't present along the entire lumen, just in some spots, compared to laminin (data not shown).

Extracellular matrix is essential for VM

VM in vitro requires Matrigel, but whether this is due to the physical requirement of a matrix for 3D growth or the presence of proteins in the Matrigel to initiate the process is unknown. To answer this question, we heated Matrigel to 65°C for 10 min, to denature any proteins present in the matrix, yet maintain a matrix in which cells could attach and grow onto. Denatured Matrigel allowed the formation of a monolayer of cancer cells but not the formation of VM structures (supplementary Fig. 4a).

We have been able to get reproducible results using Matrigel purchased from three different companies (Matrigel from Corning, Cultrex from R&D Biosystems, GelNest Matrix from Wuxi Nest Biotechnology). Furthermore, the assay is reproducible irrespective of whether we use standard Matrigel or Matrigel depleted in growth factors (both Corning). A protein-free 3D hydrogel (purchased from TheWell Bioscience) did not promote VM formation (not shown). To identify the protein(s) we utilized Matrigel that was depleted in ECM proteins except for either laminin 111 or collagen I. As shown in Fig. 4, in both cell lines and in a primary culture of patient derived ovarian cancer cells, VM formation occurs in Matrigel that contains only laminin 111, but not on a matrix that exclusively contains collagen I. Furthermore, we observed that the coating of tissue culture grade plates with recombinant laminin 111 did not facilitate the formation of VM (not shown). These results altogether demonstrate that the process requires both a 3D matrix for growth and the presence of specific matrix protein content.

Integrin β_1 and the PI3K signaling pathway are involved in the formation of VM

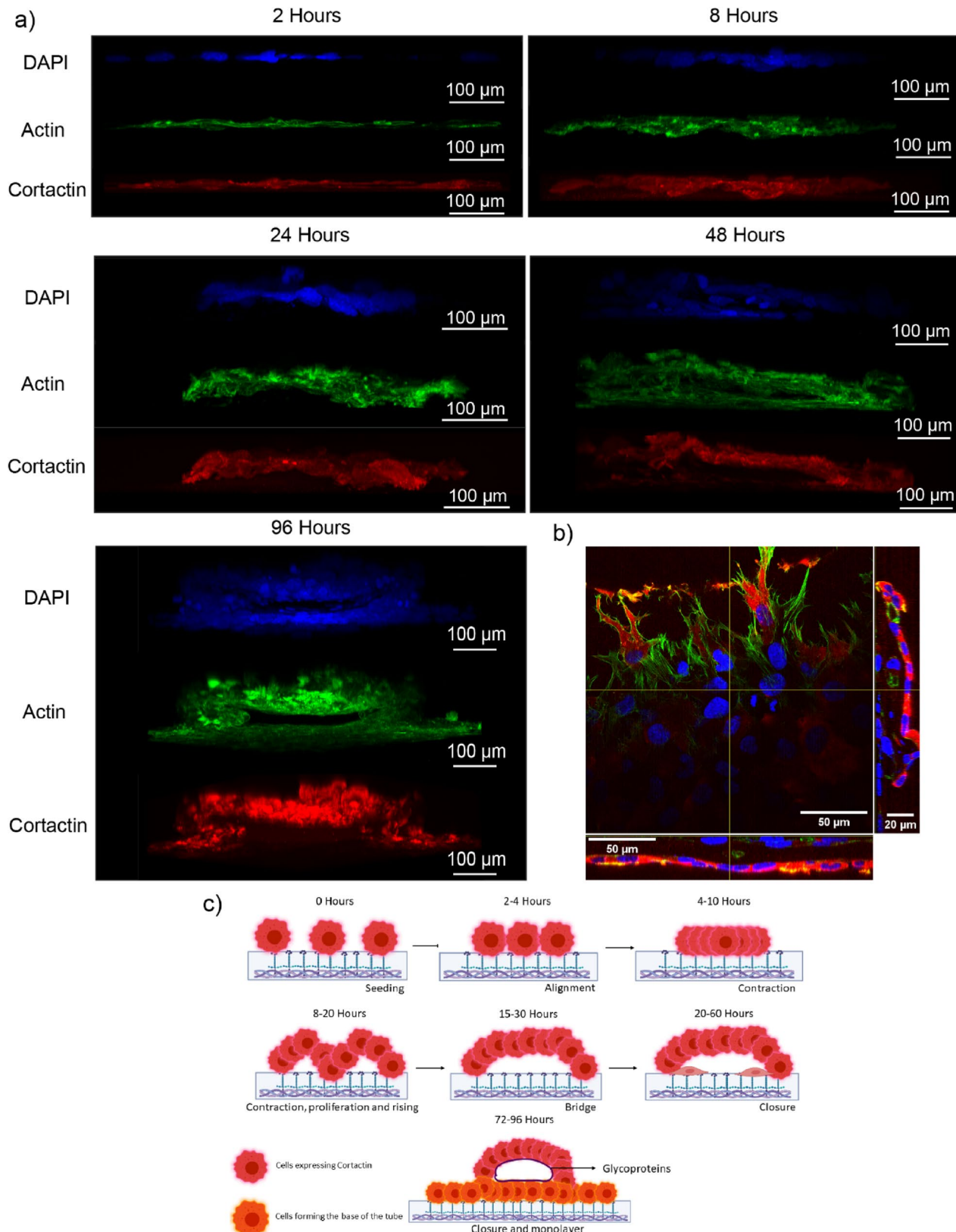
Given that the laminin 111 in the ECM is reported to signal from the matrix to the actin cytoskeletal via integrins, treatment with pharmacological inhibitor TCI-15, an inhibitor of integrins $\alpha_2\beta_1$, $\alpha_V\beta_3$, $\alpha_5\beta_1$, $\alpha_6\beta_1$, and $\alpha_{IIb}\beta_3$, blocked VM formation in both cell lines [36, 37]. Since it is the conformational change of the β subunit, the responsible for extension and activation of integrin heterodimer, we focused only on integrins β_1 and β_3 [38]. Using blocking antibodies against integrin β_1 and integrin β_3 , only the former inhibited VM formation (Fig. 5) [39, 40]. We confirmed localization of integrin β_1 at the cell membrane during VM formation and throughout the whole process in both cancer cell lines (Fig. 5C). In

accordance with previous publications in the MDA-MD-231 we confirm the specifically by siRNA knock-down of integrin β_1 which also resulted in the absence of VM structures (Fig. 6). Figures 7 shows representative immunofluorescence images of integrin β_1 (green), F-actin/phalloidin (red), and nuclei stained with DAPI (blue). An increase in integrin β_1 signal is observed during VM formation compared with cells grown as a monolayer on denatured Matrigel (Fig. 7A and B). Quantitative analysis of three independent biological experiments is presented in Fig. 7C demonstrating an increase of integrin β_1 during VM formation at 2 h. Integrin β_1 immunofluorescence is shown at 2, 8, and 24 h, with a reduction observed at 8 and 24 h (panel labbed Fig. 7D), corresponding to the graph in Fig. 7E. During the first 24 h cells remain as a monolayer, whereas by 96 h they form tubular structures. Orthogonal confocal views in Fig. 7F demonstrate that integrin β_1 expression localizes to the upper monolayer, corresponding to the original cell layer at earlier time points. Z-stack separation into bottom and middle planes reveals the two walls of the tube and a hollow lumen, with integrin β_1 expression detected at the tube closure (apical/top region) (Fig. 7G).

Downstream of integrin outside-in signaling, the PI3K pathway has been previously reported to be essential for the completion of the process of VM, however the roles of FAK and AKT have not yet been demonstrated in this in vitro model [14]. Figure 8 shows that chemical inhibition of PI3K (LY-294,002 hydrochloride (iPI3K)) hindered the VM process at early stage (before 8–12 h), however, FAK (PF-573228) and AKT (AKT inhibitor IV) inhibition allowed the aligning and connecting of the cancer cells within the first 12 h but did not allow progression to the later stages of lumen formation (as shown at the 24 timepoint in Fig. 8). Pathway inhibitors do not cause toxicity in the HEY-A8 ovarian cancer cell line as measured by the MTS and allow proliferate to a cell monolayer on Matrigel (see supplementary Fig. 3). In accordance with previous reports, we verified that VM formation requires PI3K, FAK and AKT are essential only after the initial stages (migration and connection) are complete. The conclusion that these signaling pathways are not involved at early-stage formation was confirmed by phosphoarray analysis, described in detail in legend of Fig. 8.

De novo transcription is not a principal regulator of the VM process

Taking advantage that VM can form on Matrigel, but not on denatured Matrigel, we extracted mRNA at 2, 8, 24 and 48 h from cells grown on both substrates in four independent VM experiments. The mRNA was analyzed through RNA sequencing (RNASeq) by the Beijing Genomic Institute (BGI). The formation of VM at each time point in each independent experiment is shown in

**Fig. 2** (See legend on next page)

(See figure on previous page.)

Fig. 2 Confocal microscopy demonstrating the formation of VM over time **A** HEY-A8 cells were seeded onto Matrigel and fixed at different timepoints. Immunofluorescence and analysis by confocal microscopy. 3D reconstruction of z-stacks shows first a raising (bridge structure) and the start of lumen formation at 24 h and a closed tube at 48 h to 96 h. Cortactin (red), F-actin (phalloidin, green) and the cell nucleus stained by DAPI (blue). **B** Orthogonal image (20X) of the tubular structure base at 48 h demonstrating cells migrating under the bridge structure to close the tube. **C** A schematic representation of this four-step process. Image created using Bio-Render. Representative images from a minimum of three experiments

supplementary Fig. 4B. Transcriptomics levels of cells forming VM compared to cells forming a monolayer show that depending on the time of tubular structure formation there are only a few genes that are up- or downregulated with a statistical change despite the notable change in biological phenotype. In supplementary Fig. 5 we are showing volcano plots the result of one of the four replicates. When analyzing the results of the four replicates combined, the number of regulated transcripts decreases considerably. Specifically, at 2 h of VM formation there are only 9 Genes upregulated, at 8h there is only 1 Gene downregulated, at 24h there is 1 Gene upregulated and 3 downregulated, and at 48 h there are 7 genes downregulated. In accordance, when we examine the heatmap figure in Fig. 9A comparing mRNAs in all the samples, the distribution is by time point and not than cells forming or not forming VM. Similarly, the Venn diagram in Fig. 9B compares differentially expressed genes (DEGs) between samples forming and not forming VM, in a specific replicate. Figure 9C shows the transcripts that changed at timepoints with in a specific replicate. Although the number of changes in transcripts does not necessarily relate to function, it was at the 2 h timepoint that the greatest difference was observed in cells forming or not forming VM. Gene Ontology analysis demonstrated the potential biological processes and molecular functions of the four replicates, at different timepoints of VM formation (supplementary Fig. 6). The data discussed in this publication have been deposited in NCBI's Gene Expression Omnibus [41] and are accessible through GEO Series accession number GSE263232 (<https://www.ncbi.nlm.nih.gov/geo/query/acc.cgi?acc=GSE263232>). However, albeit a low number, there were significant changes in RNA expression present in several of the four independent experiments (supplementary Table 1).

Discussion

VM has been a controversial area since the first report by the Hendrix group in 1999 [6]. This controversy is further hindered by the lack of standardization in an in vitro model to allow the discovery of meaningful biomarkers (that can be applied both in research and in the clinic) and potential new anticancer targets for this phenomenon that is correlated to poor patient survival [7]. We previously presented a model demonstrating that both primary tissues and cancer cell lines can form lumen-containing and fluid-conducting tubular structures when grown in Matrigel [9]. These tubular structures

require several days in culture and the resultant PAS-positive lumen is lined by glycoprotein of an unknown nature. Herein, we demonstrate in a breast and ovarian cancer cell line that this lumen is rich in laminin. While, in our opinion, this confocal microscope gives the first solid confirmation that the lumen is laminin lined, other authors have speculated the presence of laminin in these structures. Seftor and colleagues (2001) had previously noticed that laminin- γ 2 was increased in a VM microarray analysis [12]. Laminin networks have been suggested to associate with PAS+ structures in tumor cross sections, and laminin- γ 2 has been identified in certain assays [10, 42–45]. Herein, we have shown (Fig. 3) the very first solid evidence of the presence of laminin inside the tubes formed by breast and ovarian cancer cell lines during VM. Our identification of laminin as a lumen lining further confirms that these VM structures are not lined directly by cells, thus further proving the structural difference between VM and endothelial-lined blood vessels. Vascular structures of this nature have only been identified in invertebrates and speculated in trophoblastic cells forming the placenta [7].

Center to the controversy in this field is the use of the intercellular connections after 24 h on Matrigel as an indicator of in vitro VM. Our current publication puts this dilemma into perspective, as we show that an initial aligning, migration, and intercellular interaction is merely the first of four steps that are required to produce a lumen. As we demonstrated previously, a high percentage of immortalized cells and primary cancer tissue form connections in the first 24 h, however these structures often do not continue into lumen containing tubular structures that are capable of fluid conduction [7]. In deciding whether quantitation of this assay is possible using Image J, as published by authors, given our current knowledge of VM, our conclusion is that it cannot be at the present time. For this reason, we have characterized the process of VM into four distinct phases. How do we define VM in vitro? The answer our group propose is the formation of tubular structures with the presence of a lumen on an extracellular matrix substrate (e.g. Matrigel). As outlined in what we define as step 1, the simple cellular connections at this stage may form VM or may not, depending on the specific cancer cells under investigation. Do longer, thicker or more honeycomb patterns form better future VM structures? Current knowledge does not enable us to answer this question and thus we cannot use this as a method to quantify. Even at further

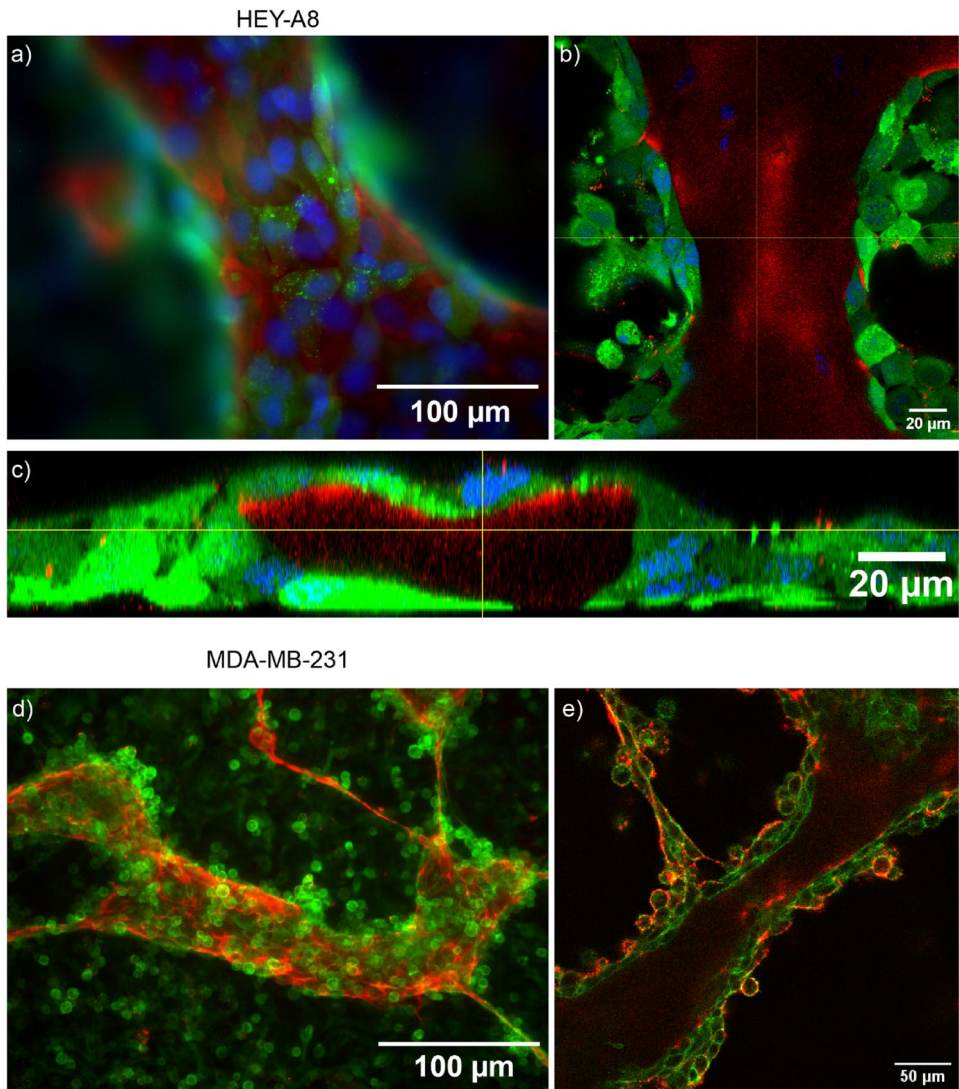


Fig. 3 The luminal lining of VM vessel is rich in laminin. **A** Epifluorescence demonstrating the presence of pan-laminin immunoreaction below the cancer cell layer in the HEY-A8 cancer cell line. Pan-laminin (red), cancer cells transfected with fluorescent protein (green) with the cell nuclei stained by DAPI (blue). **B** and **C** Orthogonal view from a z-stack showing the walls of the tubular structure and pan-laminin immunoreaction in the lumen. Pan-laminin (red) immunoreaction within the lumen wall. **D** Epifluorescence demonstrating the presence of pan-laminin immunoreaction below the cancer cell layer in the MDA-MB-231 cancer cell line. Pan-laminin (red) and F-actin (phalloidin, green). **E** Still image taken from Z-stack reconstruction showing the walls of the tubular structure and pan-laminin immunoreaction (red) and F-actin (phalloidin, green). Representative images from a minimum of three experiments in each cell line

stages of VM, tubular structures vary in both width and length. In accordance, a wide range of vessel diameters have been observed by pathologists in tumor patient cross sections. Until we understand this process better and potentially follow VM progression through a specific marker protein, herein we have proposed a four-step process to help report at what stage VM reaches in the presence of an inhibitor or an environmental change. While the role of FAK in VM has been speculated previously [46], we can now report that FAK is not essential for the first step of VM, i.e. a network of interconnecting cells is present in a cell line shown to form lumen containing structures at later time points. However, FAK protein is

essential for at least the second stage of VM as formation stopped before the 24-hour time point (probably between 8 and 12 h) having only presented intercellular connections. In contrast, the knockdown of integrin $\beta 1$ inhibits all stages of VM formation and thus is responsible in the initiation of the structures. Interestingly, Kawahara and colleagues had reported previously by intergrin $\beta 1$ deletion, then rescue experiments, that integrin $\beta 1$ is responsible for allowing the intercellular connections present when the MDA-MB-231 cells were grown on Matrigel [47]. Our results confirm this observation in the breast cancer cell line, and demonstrate that the formation of tubular stuctures at 4 days in the both the MDA-MB-231

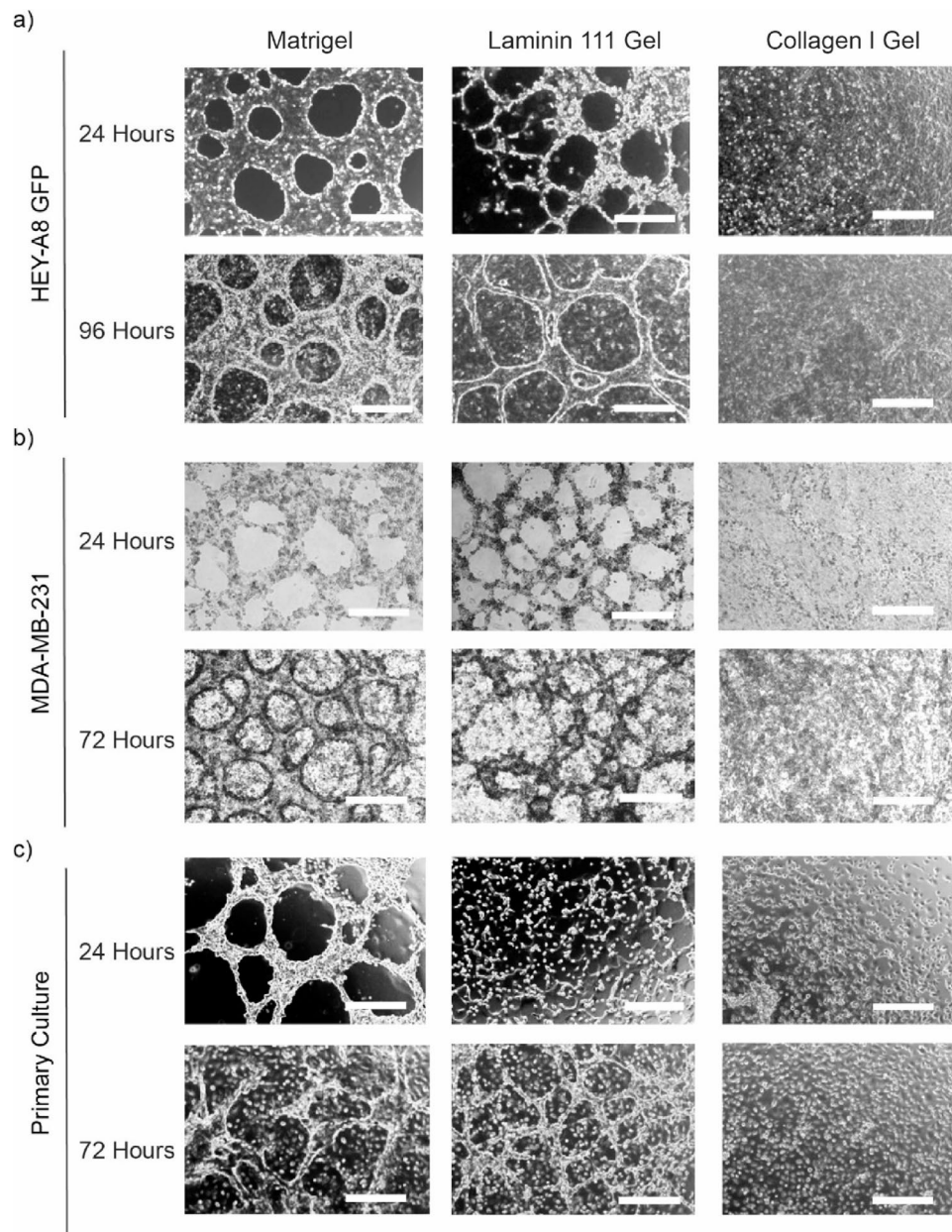


Fig. 4 Matrix of laminin 111 is sufficient to allow the process of VM HEY-A8 GFP (**A**), MDA-MB-231 (**B**) and primary cultured ovarian cancer cells (PC) were grown on Matrigel or Gels composed in either laminin 111 or collagen I for 24 and 96 h. Cells seeded in either Matrigel or the Gel composed only by laminin 111 form VM, while cells seeded in gel only composed by collagen I do not form VM. Scale bar = 100 μ m. Representative images from a minimum of three experiments in each cell line, and one patient sample

and HEY-A8 cell line require the presence of integrin $\beta 1$, but not intergrin $\beta 3$. Knowing that integrin $\beta 1$ is essential for formation from the first stage we examined the temporal expression profile of this protein. Integrin $\beta 1$ had higher expression in cells forming VM than cells forming a monolayer on denatured Matrigel. Interestingly, this initial expression fell at 8 and 24 h, potentially suggesting that the integrin role is required for the initiation of the VM process. This hypothesis is supported by our observation that the absence of natural Matrix proteins

(an example being laminin 111) also results in a failure to initiate this process. A further interesting observation was that integrin $\beta 1$ was more abundantly expressed in the upper layer of the tubular structure at 96 h. This is in keeping with our earlier results showing that the monolayer of cells at 24 h is elevated (bridge structure) and this forms the top of the vasculogenic mimicry tube. Future experiments may show a functional role for the localization of this and other proteins in the functionality of these tubes. In future publications, we encourage authors

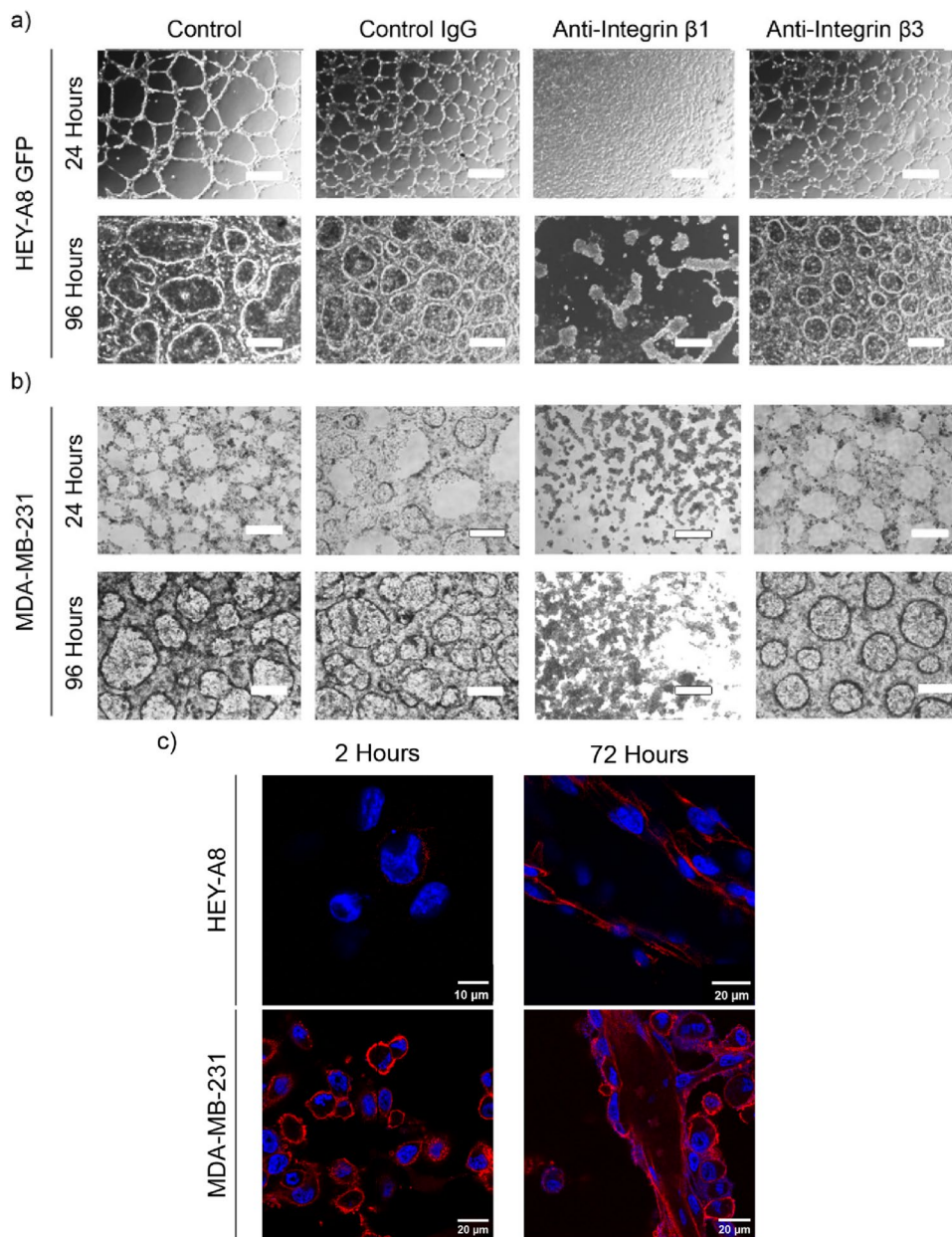


Fig. 5 Integrin β 1, but not integrin β 3, is required for the formation of VM HEY-A8 GFP (**A**) or MDA-MB-231 (**B**) cells were incubated with a blocking antibody against integrin β 1 or integrin β 3 before seeding on Matrigel for 96 h. Photographs were taken at 24 and 96 h. Blocking of integrin β 1 is enough to stop the formation of VM. (**C**) Airy Scan microscopy demonstrating the presence of integrin β 1 (red) and the cell nucleus stained by DAPI (blue) in both cell lines during VM formation at 2 and 72 h. Scale bar = 100 μ m. Panel A & B, representative images from a minimum of three experiments in each cell line. Panel C representative images from two experiments

to demonstrate that any report on in vitro VM is accompanied by clear evidence of a lumen-containing structure and not just intercellular connections at 24 h.

As mentioned above, the PI3K pathway is crucial for completion of the VM process, however, the individual inhibition of FAK or AKT does allow the migration and intercellular connections in step 1 of VM, but then the process stops, and the later stages of lumen formation do not occur [9, 14, 48]. This demonstrates that the

VM process requires specific components of the PI3K pathway at specific time points. Although only showing (potentially) initial stages of VM, several papers have shown an involvement of AKT during VM formation and others have reported a decrease in FAK and AKT when VM was inhibited [10, 49]. In agreement with our chemical inhibition of FAK not inhibiting VM formation before 12–24 h, no phosphorylation of Tyr407, Tyr576, Tyr861, Tyr925 or Tyr397 (essential for FAK activity),

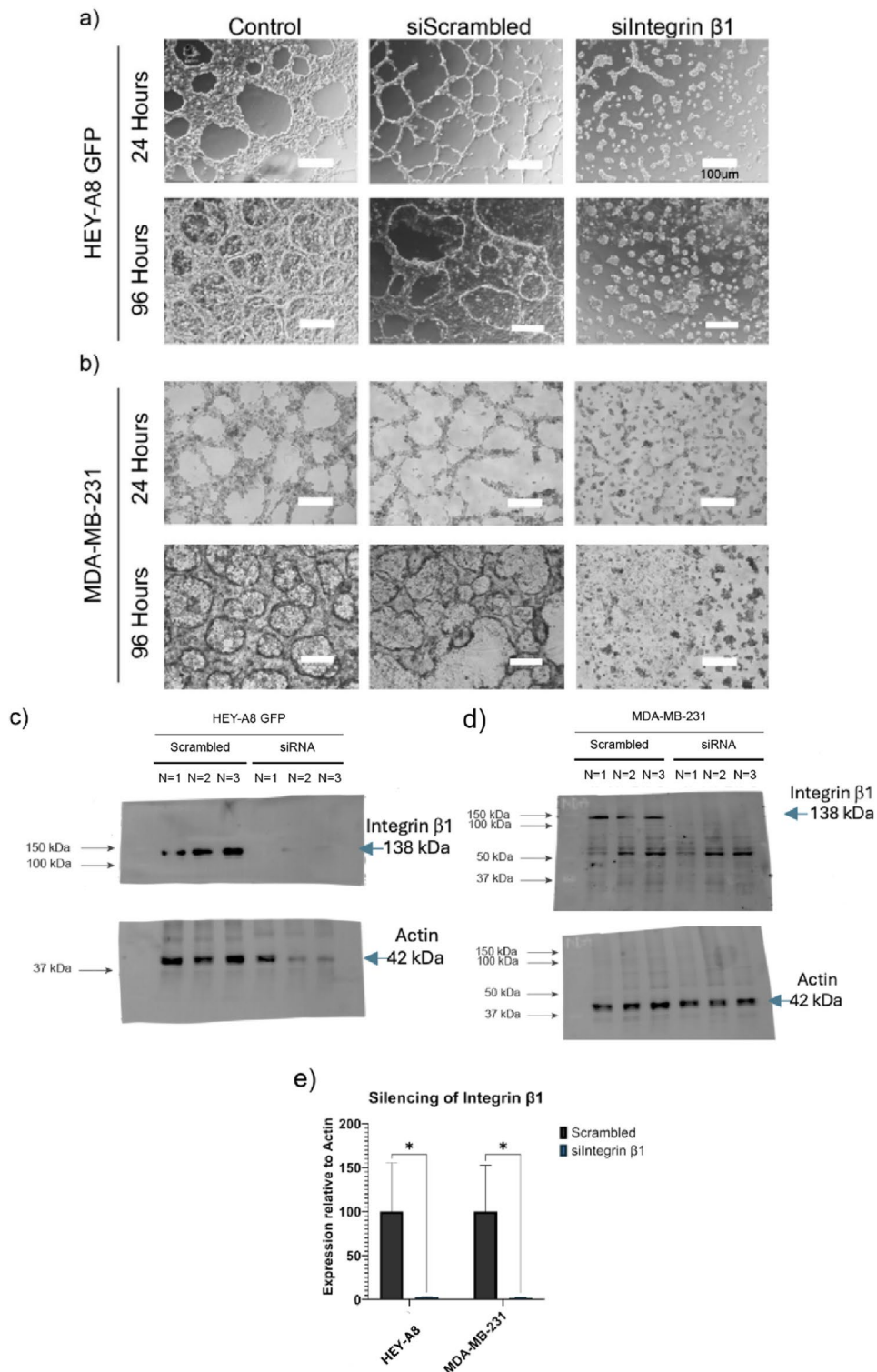


Fig. 6 Integrin $\beta 1$ is essential for the formation of VM HEY-A8 (**A**) or MDA-MB-231 (**B**) cells were transfected with siScrambled or siRNA against integrin $\beta 1$ (silIntegrin $\beta 1$) before seeding on Matrigel for 96 h. Photographs were taken at 24 and 96 h. Cells that were transfected by silIntegrin $\beta 1$ do not form VM. (**C-E**) Western blot demonstrates that levels of integrin $\beta 1$ protein were reduced. * = $p < 0.05$. Scale bar on panel A = 100 μ m. Representative images from a minimum of three experiments in each cell line

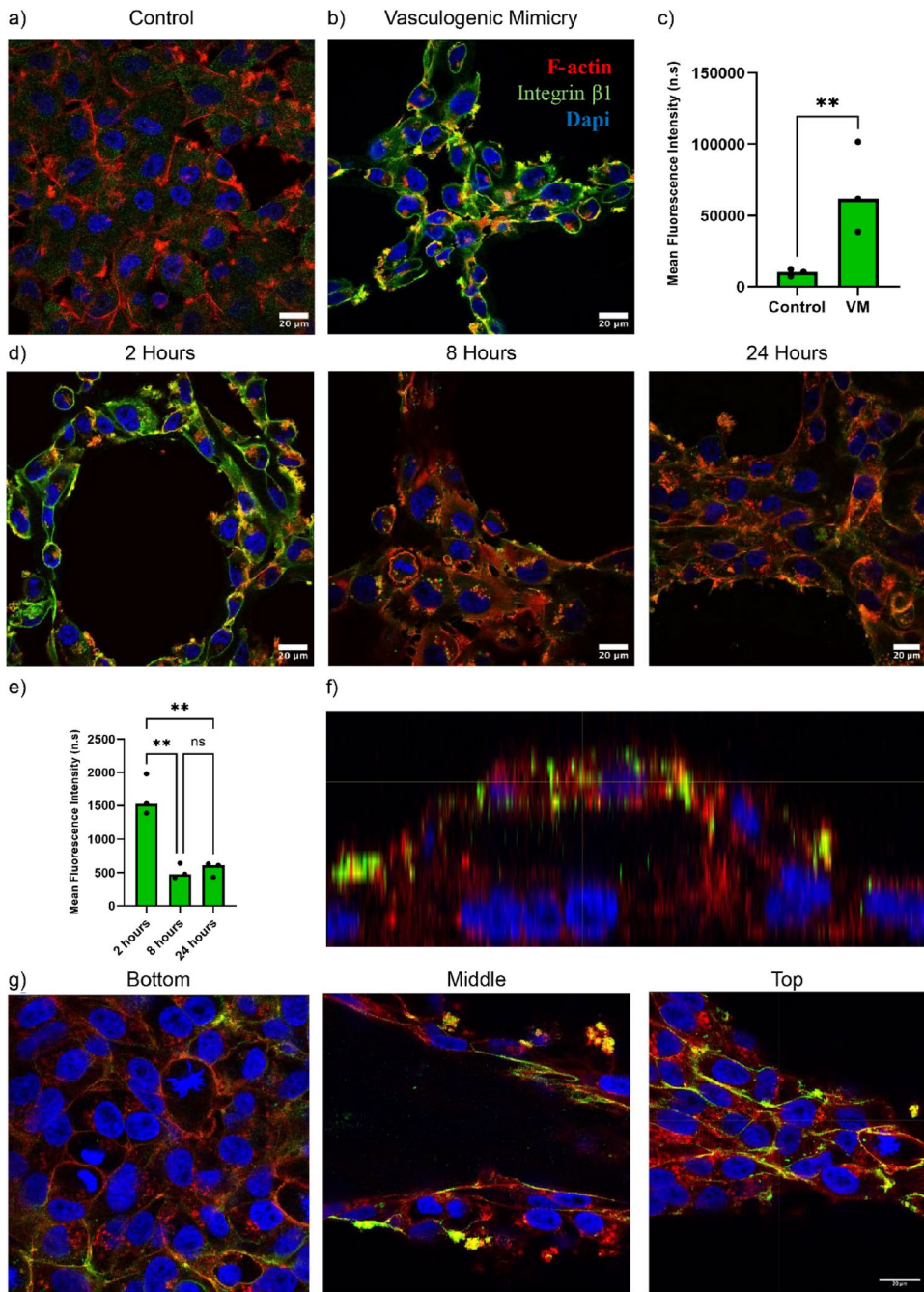
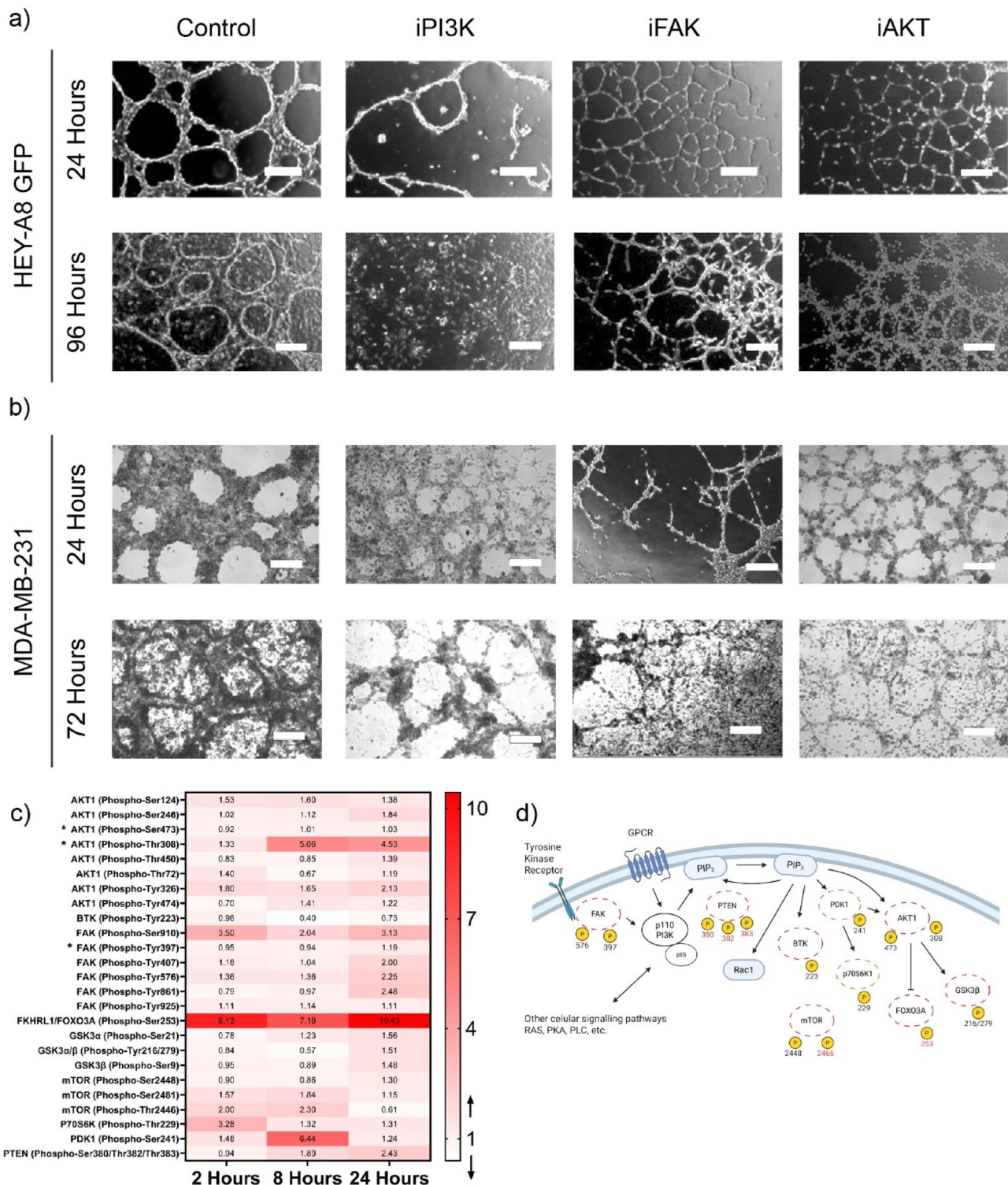


Fig. 7 Integrin β1 is highly expressed and localized on the plasmatic membrane during VM formation **A** and **B** Confocal microscopy showing that integrin β1 is localized in the plasmatic membrane of HEY-A8 cells at 2 h of VM formation. **(C)** Quantification of integrin β1 intensity comparing cells grown on denatured Matrigel (control) and cells grown onto Matrigel after 2 h (VM). **D** HEY-A8 cells were seeded onto Matrigel and fixed at different timepoints. Confocal microscopy shows that integrin β1 is highly localized at 2 h of VM formation but not at 8 and 24 h. **E** Quantification of integrin β1 intensity comparing different timepoints of VM formation. **F** 3D reconstruction of z-stacks showing that integrin β1 is localized at the top of the VM tube at 96 h. **G** Confocal microscopy showing that integrin β1 is more present at the top of the VM tubular structure compared to the bottom and the middle of the tube. For all images integrin β1 (red), F-actin (green) and the cell nucleus stained by DAPI (blue). Representative images from a minimum of three experiments in each cell line. * = $p < 0.05$.

was observed a 2–8 h of VM formation. Interestingly Ser910, an understudied phosphorylation thought to be involved in mediating various signal pathway interactions was phosphorylated at these early time points,

although our results may suggest that this phosphorylation is not essential in early stage VM [50–54]. While no change occurred in the essential FAK phosphorylation at Tyr397, at 24 h there was an increase in Tyr407,

**Fig. 8** (See legend on next page.)

Tyr576 and Tyr861 at 24 h and these remain to be tested in future experiments to verify if these play an essential role in VM formation and thus the reason why VM formation stops in early stage with a FAK inhibitor. AKT is

activated by dual phosphorylation at Thr308 and Ser473, reportedly due to an activation of PDK1 when being phosphorylated at Ser241 [55, 56]. Even though there is an increase in the phosphorylation of Thr308 at 8 and 24

(See figure on previous page.)

Fig. 8 The PI3K-FAK-AKT pathway is required for the formation of VM HEY-A8 **A** or MDA-MB-231 **B** cells were seeded on Matrigel for 96 hours. 1 hour after seeding cells were treated with LY-294002 hydrochloride (20 μ M, iPI3K), PF-573228 (400nM, iFAK) or AKT inhibitor IV (625nM, iAKT). Treatments were replenished after 48 hours. Photographs were taken at 24 and 96 hours. Inhibition of PI3K inhibits stages early on in VM formation in HEY-A8 cells, but in MDA-MB-231 inhibition occurs after the first step of migration and aligning (aprox 8-12hours). The latter also occurs with the inhibitor of FAK or AKT in both cell lines. Scale bar = 100 μ m. Representative images from a minimum of three experiments. **C** HEY-A8 cells were seeded on Matrigel or denatured Matrigel for 2, 8 and 24 hours. Protein lysate was extracted at 2, 4 and 24 hours and sent to Full Moon BioSystems to be analyzed by a Phospho Explorer Antibody Array. From the data obtained a heatmap was generated showing changes in phosphorylation of selected proteins related to the PI3K-FAK-AKT pathways. **D** Schematic PI3K-FAK-AKT pathways during the first 24 hours VM formation. The proteins not activated according to our phosphorylation array are indicated by red circles, while green circles denote proteins that are phosphorylated at the specified sites (black numbers) and therefore considered activated. Red numbers represent phosphorylation that reduce the enzymatic activating the protein. Notably, changes in full activating phosphorylations* of FAK (Thr397) and AKT (together Ser 308 and Ser 473) are not observed during the first 24 hours of VM formation. Activating phosphorylation of Phosphatase and Tensin Homolog deleted on chromosome 10 (PTEN) at site 380 favors the formation of PIP3. Interestingly, other downstream components of the PI3K pathway—such as mammalian target of rapamycin (mTOR), Forkhead Box O3a protein (FOXO3a), also have increased phosphorylation on sites that reduce the activity of these proteins. There is downregulation of phosphorylation at Tyr223 on Bruton's tyrosine kinase (BTK) which is a critical regulatory modification that enhances the enzyme's catalytic activity. A similar situation is seen with phosphorylation at tyrosine 216 (Tyr216) on glycogen synthase kinase-3 beta (GSK-3 β). Conversely activating phosphorylation is observed on other phosphoinositide 3,4,5-trisphosphate (PIP3) associated proteins such as 3-phosphoinositide-dependent protein kinase-1 (PDK1) Ser241 and p70S6K1 Thr229 (albeit not at the same time point). These observations add to the conclusion that AKT and FAK are not essential in the initial stages of VM. Created in BioRender.

h of VM formation, which correlates positively with an increase phosphorylation of PDK1 in Ser241, there are no changes in Ser473, possibly indicating that AKT is not fully activated and again agreeing with our observation that chemical inhibition of AKT does not alter early VM formation. Also in accordance is the phosphorylation at 8 and 24 h of PTEN at Ser380, Thr382 and Thr383 which leads to loss of phosphatase activity and tumor suppressor function, and coincides with an increase in phosphorylation of AKT at Thr308 [57]. Future phospho-mutant experiments will ascertain if Thr308 at 8 and 24 h is essential for VM. In summary, at early time points AKT and FAK are not fully activated, potentially explaining why AKT and FAK chemical inhibition does not affect VM formation before 12–24 h. The ability of chemical inhibition of PI3K to eliminate all VM may suggest that formation of PIP₃ is required, potential activation of PDK1 at Ser241 and downstream targets such as phosphorylation of p70S6K are required in VM formation. However, the PI3K subunits also feed into the RAC and other pathways such as Ras, PKA and PLC. Experiments are ongoing with further chemical inhibitors and phospho-mutant proteins to answer these questions and understand the complex signaling involved in the four phases of VM formation.

Integrin β 1 is essential for VM and is present at the cell membrane during the entire four-day process. This further confirms results that show in non-endocrine derived CDX30P cancer cells the requirement of integrin β 1 to form hollow tubules at 72 h [13]. Furthermore, Liu and colleagues (2021) showed by fluorescent staining in MDA-MB-231 that integrin β 1 localized to the cell surface during what appears to be the initial stages of in vitro VM [58]. These authors also observed alterations in glycosylation of integrin β 1. In support of integrin β 1 as a potential VM biomarker, immunohistochemistry staining has suggested that integrin β 1, together with nectin-4,

is associated with VM formation and distant metastasis [59].

Although further experimentation is required to show cause and effect, our results suggest that integrin β 1 may be initiating the process of VM by connecting to laminin 111 in the ECM (Matrigel). Our depletion experiments show that the presence of laminin 111 in hydrogel (commercially available depleted Matrigel) is sufficient to allow VM. A similar collagen I-containing depleted Matrigel did not permit VM formation (although attachment and proliferation occurred). This may have logic, as in the basement membrane it is laminin, not collagen, that is nearest to the cell and forms connections through integrins. Although not shown, when we mixed a non-protein containing hydrogel with recombinant laminin 111, we did not see VM formation, suggesting that laminin is required either in a specific conformation (potentially cross-linked) or a yet unidentified matrix component is required. Interestingly, laminin 111 is abundant in tumors and during embryogenesis, but is not common in the adult body. While no solid evidence is available, we speculate that the cancer cell may create its own microenvironment (Matrigel is derived from a sarcoma) rich in laminin 111 and this embryogenic signal may trigger signaling pathways destined to tubular structure formation. The α chains of laminin 111 binds to integrins $\alpha 1\beta 1$, $\alpha 3\beta 1$, $\alpha 4\beta 1$, $\alpha 6\beta 1$, and in accordance, our experiments demonstrate that it is integrin β 1 not integrin β 3 that is essential [60]. The future knockdown of individual integrin subunits may provide more precise information on the mechanism of action. Although not addressed herein, the authors are aware that denaturing the Matrigel not only denatures proteins but may have a mechanobiology effect of changing the stiffness of the Matrigel. Future experiments will be needed to determine the role of stiffness in the presence and absence of natured matrix proteins.

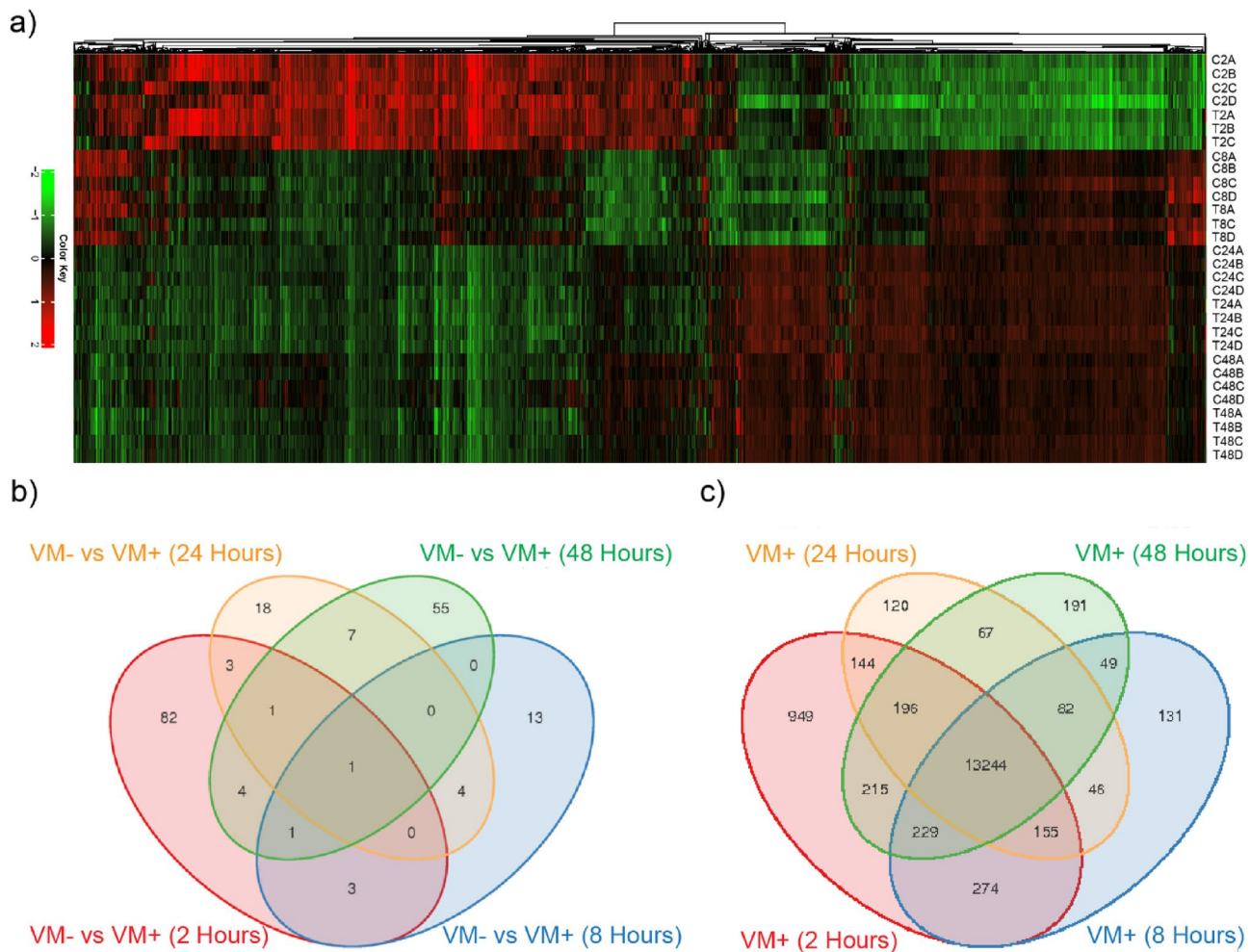


Fig. 9 Multiomics analysis and validation by time and presence of VM. HEY-A8 GFP cells were seeded on Matrigel or denatured Matrigel for 2, 8, 24 or 48 hours. RNA was extracted and sent to BGI Genomics in Hong Kong to be analyzed by RNASeq. **A** From the data obtained a heatmap was generated using iDEP where it can be seen that the differences between up and downregulated genes is in the time when the samples were obtained rather than the formation of VM [68]. **B** Venn diagram of the third replicate comparing the DEGs between cell forming or not forming VM. **C** Venn diagram showing the genes that were present at each timepoint from the third replicate

Given the striking biological observation that tubular structures are present on Matrigel but absent on denatured Matrigel, it came as a surprise that our RNASeq analysis revealed only 11 genes that were altered in a majority of four separate biological replicates ($N=4$). Interestingly, under similar conditions and number of replicates, a microarray in gastric cancer (results not shown) returned a similar number of significantly altered genes (albeit different). This result suggests that the process of VM is regulated principally at the post-transcriptional level. In accordance, the alignment of cancer cells on Matrigel occurs within 15 min, and the first cell interactions within the hour, which is potentially too quick for the majority of transcriptional responses. However, current dogma still implies that the formation of tubular structures over a 4-day period requires transcriptional regulation different to that of cell survival and

proliferation. We observe that the VM process always occurs in four distinct stages and is complete within 4 days, however depending on the experiment, step 2 may occur as early as 8 h and as late as 20 h. It is this interexperimental difference at 2, 8, 24 and 48 h that may cause sufficient changes in RNA for statistical significance to be lost when four biological replicates are considered. Interestingly, work from the group of López-Camarillo in MDA-MB-231 reported that a miR-204 and miR-145 mimics resulted in the inhibition of the early stages of VM formation [61, 62]. It is thus likely that transcriptional changes are present and necessary for VM, however we should also focus on post-transcriptional and post-translational signaling pathways. As expected, phosphoarray data shows that phosphorylation occurs during VM formation.

We are aware of the potential limitations that an in vitro model possesses. The aim of our experimentation is to identify a key protein (or modified protein) in VM formation that will serve as a biomarker of VM and thus replace the currently inadequate identification by the absence of CD31. Once this marker has been identified, the positive staining by immunohistochemistry in tumor slides will validate that this in vitro model corresponds to VM presence in tumors. In vivo the TME plays an essential role in tumor development through interactions between other cell types, such as fibroblasts, endothelial and immune cells [63]. Even the composition of the ECM that is found on the TME has a critical role in tumor progression [64]. Our in vitro model utilizes Matrigel, a commercially ECM extracted from Engelbreth-Holm-Swarm mouse tumor, which composition is 60% laminin, 30% collagen IV, and 8% nidogen/entactin [65, 66]. We demonstrate that Laminin 111 alone permits the formation of VM, however, this does not rule out that other matrix proteins can also have a similar effect. Furthermore, this model does not consider the role and contribution of other cell types present within the TME, such as fibroblast, inflammatory and immune cells, blood vessels and even the microbiome. Standard deficiencies of an in vivo model aside, herein we believe that we demonstrate the most comprehensive in vitro model to date of the formation of lumen-containing and fluid-conducting tubular structures comprised exclusively of cancer cells. We hope that this model, and the supplied RNASeq data, will help identify biomarkers of VM containing tumors and identify druggable targets to offer a better quality of life to patients with these aggressive tumors.

Conclusions

The contribution of our results to the vasculogenic mimicry community has been to define that the VM process occurs in four distinct stages: (1) alignment, migration then clustering delineate the area of the future tubular structure. (2) contraction of aligned multilayer structures followed by reorientation of some cells and cellular blebbing. (3) mass proliferation followed by the raising of specific areas of the cancer cell mass above the Matrigel (bridge). (4) the formation of a cell monolayer at the Matrigel surface that closes the tubular structure, forms a laminin-rich luminal lining, then further elevates the structure. We anticipate that these steps will be further subdivided in the future. Many other factors may be involved in the formation of VM that are not included in this model. Interestingly a recent paper speculated on the role of the immune system in this process [67]. While presenting solid arguments as to why this assay cannot be justifiably quantified using imageJ software, we do present a manner that will allow the discussion of quantification. We demonstrate that the four stages utilize different

signaling pathways, with matrix proteins and Integrin $\beta 1$ being essential from the initiation of VM, while inhibitory PI3K/AKT/FAK chemicals showing varying degrees of antagonism at later stages.

After much speculation in the literature regarding the role of the ECM, herein we conclusively demonstrate that the matrix not merely provides a 3D environment but also contributes specific proteins (we show that laminin 111 is one such protein) that are required to initiate this process. Furthermore, after numerous reports suggesting the involvement of integrin $\beta 1$ and the structural presence of laminin, we demonstrated by siRNA the essential nature of this integrin, and that laminin is lining the lumen of the tubular structure. Our RNASeq analysis raised more questions than it answered, however, we now conclude that the regulation pathway of VM is predominantly post-transcriptional/translation. Current studies are ongoing to perform a comprehensive phospho-array analysis. Preliminary results from this analysis show that full activation of the AKT and FAK signaling pathways are not essential for early stage VM formation. We have observed that differences exist in the process of VM formation between our two reported cell lines (and further cancer cell lines and primary cultures studies within our laboratory), that suggests there may be either redundancy within protein families mediating VM and/or there is more than one route to obtain tubular structures. This highlights the current difficulty in finding a highly specific biomarker of VM for clinical use. Hopefully, our characterization of an in vitro VM model and the presentation of new pathways and proteins will help identify both a future marker of VM and potentially druggable targets to treat the VM-containing subtype of cancer tumors, which notably correlates with poor patient prognosis.

Supplementary Information

The online version contains supplementary material available at <https://doi.org/10.1186/s12964-025-02428-0>.

- Supplementary material 1.
- Supplementary material 2.
- Supplementary material 3.
- Supplementary material 4.
- Supplementary material 5.

Acknowledgements

We acknowledge all the help of the microscopy platform at the Pontificia Universidad Católica de Chile, especially Nicole Salgado and Fernanda Garate. Furthermore, we are grateful for the generosity of the patients who donated their cancer to this research.

Authors' contributions

GM, AV, GNS, NB, VA, JP, PG, CC, JT, MV, and FN contributed to the experimentation, microscopy, and analysis. CI and RG contributed to the selection, recruitment, and analysis of the primary tissue for cell culture. JCR,

AR, CB and GLO were responsible for the design, analysis, and preparation of the manuscript.

Funding

This work was supported by ANID-FONDAP-15130011(APOYO 1523A0008) & 152220002, PROGRAMA ICM-ANID, ICN2021_045, ANID FONDECYT 1250073, 1220586, 1230983, 1221147 & 1210872, ANID-EQM210020 & EQM210101, PUC-VRI-Puente-2022-13, FONDEQUIP EQM170188, Núcleo Milenio SELFO NCN2024_068

Data availability

The RNA data is available on: [<https://www.ncbi.nlm.nih.gov/geo/query/acc.cgi?acc=GSE263232>] (<https://www.ncbi.nlm.nih.gov/geo/query/acc.cgi?acc=GSE263232>).

Declarations

Competing interests

The authors declare no competing interests.

Author details

¹Department of Physiology, Faculty of Biological Sciences, Pontificia Universidad Católica de Chile, Santiago, Chile

²Department of Hematology and Oncology, Faculty of Medicine, Pontificia Universidad Católica de Chile, Santiago, Chile

³Department of Pathology, Faculty of Medicine, Pontificia Universidad Católica de Chile, Santiago, Chile

⁴Institute for Biological and Medical Engineering, Schools of Engineering, Medicine and Biological Sciences, Pontificia Universidad Católica de Chile, Santiago, Chile

⁵Centro de Biología Celular y Biomedicina (CEBICEM), Facultad de Ciencias, Universidad San Sebastián, Santiago, Chile

⁶Center for Advanced Clinical Research (CICA), Department of Neurology & Neurosurgery, Faculty of Medicine, Universidad de Chile, Santiago, Chile

⁷Advanced Scientific Equipment Network (REDECA), Faculty of Medicine, Universidad de Chile, Santiago, Chile

⁸Fundación Oncomujer, Santiago, Chile

⁹Center for Cancer prevention and Control (FONDAP-CECAN), Pontificia Universidad Católica de Chile, Santiago, Chile

¹⁰Faculty of Biological Sciences, NeuroCellIT and Center For Advanced Microscopy (CMA), University of Concepcion, Concepcion, Chile

¹¹Centro Ciencia & Vida, Fundación Ciencia & Vida, Santiago, Chile

¹²Graduate School of Engineering Science, University of Osaka, Osaka, Japan

¹³Advanced Center for Chronic Diseases (FONDAP-ACCDIS), Pontificia Universidad Católica de Chile, Santiago, Chile

¹⁴Millennium Institute on Immunology and Immunotherapy, Santiago 8331150, Chile

¹⁵Departamento de Ciencias de la Salud Universidad de Aysén Coyhaique, Coyhaique, Chile

Received: 25 March 2025 / Accepted: 2 September 2025

Published online: 08 October 2025

References

1. Hanahan D, Weinberg RA. Hallmarks of cancer: the next generation. *Cell*. 2011;144:646–74. <https://doi.org/10.1016/j.cell.2011.02.013>.
2. Barnett FH, Rosenfeld M, Wood M, Kiosses WB, Usui Y, Marchetti V et al. Macrophages form functional vascular mimicry channels in vivo. *Sci Rep* [Internet]. 2016;6:36659. Available from: <http://www.nature.com/articles/srep36659>
3. Zhou Y, Fisher SJ, Janatpour M, Genbacev O, Dejana E, Wheelock M, et al. Human cytrophoblasts adopt a vascular phenotype as they differentiate: a strategy for successful endovascular invasion? *J Clin Invest*. 1997;99:2139–51.
4. Rai A, Cross JC. Development of the hemochorial maternal vascular spaces in the placenta through endothelial and vasculogenic mimicry. *Dev Biol*. 2014;387:131–41. <https://doi.org/10.1016/j.ydbio.2014.01.015>.
5. Muñoz-Chápuli R, Carmona R, Guadix JA, Macías D, Pérez-Pomares JM. The origin of the endothelial cells: an evo-devo approach for the invertebrate/vertebrate transition of the circulatory system. *Evol Dev*. 2005;7:351–8.
6. Maniotis AJ, Folberg R, Hess A, Seftor EA, Gardner LM, Pe'er J et al. Vascular channel formation by human melanoma cells in vivo and in vitro: vasculogenic mimicry. *Am J Pathol* [Internet]. 1999;155:739–52. Available from: <https://pubmed.ncbi.nlm.nih.gov/10487832/>
7. Valdivia A, Mingo G, Aldana V, Pinto MP, Ramirez M, Retamal C, et al. Fact or fiction, it is time for a verdict on vasculogenic mimicry? *Front Oncol*. 2019;9:1–14. <https://doi.org/10.3389/fonc.2019.00680>.
8. Zhang L, Ding P, Lv H, Zhang D, Liu G, Yang Z, et al. Number of polyploid giant cancer cells and expression of EZH2 are associated with VM formation and tumor grade in human ovarian tumor. *BioMed Res Int*. 2014. <https://doi.org/10.1159/2014/903542>.
9. Racordon D, Valdivia A, Mingo G, Erices R, Aravena R, Santoro F, et al. Structural and functional identification of vasculogenic mimicry in vitro. *Sci Rep*. 2017. <https://doi.org/10.1038/s41598-017-07622-w>.
10. Mitra D, Bhattacharyya S, Alam N, Sen S, Mitra S, Mandal S, et al. Phosphorylation of EphA2 receptor and vasculogenic mimicry is an indicator of poor prognosis in invasive carcinoma of the breast. *Breast Cancer Res Treat*. 2020;179:359–70. <https://doi.org/10.1007/s10549-019-05482-8>.
11. Sood A, Seftor EA, Fletcher MS, Gardner LM, Heidger PM, Buller RE et al. Molecular determinants of ovarian cancer plasticity. *Am J Pathol* [Internet]. 2001;158:1279–88. Available from: <http://www.pubmedcentral.nih.gov/articlerender.fcgi?artid=1891929&tool=pmcentrez&rendertype=abstract>
12. Seftor REB, Seftor EA, Koshikawa N, Meltzer PS, Gardner LMG, Bilban M, et al. Cooperative interactions of laminin 5 γ 2 chain, matrix metalloproteinase-2, and membrane type-1-matrix/metalloproteinase are required for mimicry of embryonic vasculogenesis by aggressive melanoma. *Cancer Res*. 2001;61:6322–7.
13. Pearsall SM, Williamson SC, Humphrey S, Hughes E, Morgan D, García Marqués FJ, et al. Lineage plasticity in SCLC generates non-neuroendocrine cells primed for vasculogenic mimicry. *J Thorac Oncol*. 2023;18:1362–85. <https://doi.org/10.1016/j.jtho.2023.07.012>.
14. Hess AR, Seftor EA, Seftor REB, Hendrix MJC. Phosphoinositide 3-kinase regulates membrane type 1-matrix metalloproteinase (MMP) and MMP-2 activity during melanoma cell vasculogenic mimicry. *Cancer Res*. 2003;63:4757–62.
15. Theocaris AD, Skandalis SS, Gialeli C, Karamanos NK. Extracellular matrix structure. *Adv Drug Deliv Rev*. 2016;97:4–27. <https://doi.org/10.1016/j.addr.2015.11.001>.
16. Bonnans C, Chou J, Werb Z. Remodelling the extracellular matrix in development and disease. *Nat Rev Mol Cell Biol*. 2014;15:786–801. <https://doi.org/10.1038/nrm3904>.
17. Younis LF, Di Russo J, Sorokin L. Laminin isoforms in endothelial and perivascular basement membranes. *Cell Adhes Migr*. 2013;7:101–10.
18. Hallmann R, Hannocks MJ, Song J, Zhang X, Di Russo J, Luik AL, et al. The role of basement membrane laminins in vascular function. *Int J Biochem Cell Biol*. 2020;127:105823. <https://doi.org/10.1016/j.biocel.2020.105823>.
19. Chastney MR, Conway JRW, Ivaska J. Integrin adhesion complexes. *Curr Biol*. 2021;31:R536–42.
20. Desgrange JS, Cheresh DA. Integrins in cancer: biological implications and therapeutic opportunities. *Nat Rev Cancer* [Internet]. 2010;10:890–890. Available from: <http://www.nature.com/doifinder/https://doi.org/10.1038/nrc2965>
21. Noorolyai S, Shajari N, Baghbani E, Sadreddini S, Baradaran B. The relation between PI3K/AKT signalling pathway and cancer. *Gene*. 2019;698:120–8. <https://doi.org/10.1016/j.gene.2019.02.076>.
22. Badilloo M, Esmaeili-Mahani S. Phosphatidylinositol 3-kinases inhibitor LY294002 potentiates the cytotoxic effects of doxorubicin, vincristine, and etoposide in a panel of cancer cell lines. *Fundam Clin Pharmacol*. 2014;28:414–22.
23. Sato M, Kawana K, Adachi K, Fujimoto A, Yoshida M, Nakamura H, et al. Targeting glutamine metabolism and the focal adhesion kinase additively inhibits the mammalian target of the Rapamycin pathway in spheroid cancer stem-like properties of ovarian clear cell carcinoma *in vitro*. *Int J Oncol*. 2017;50:1431–8.
24. Gwak H, Haegeman G, Tsang BK, Song YS. Cancer-specific interruption of glucose metabolism by resveratrol is mediated through inhibition of Akt/GLUT1 axis in ovarian cancer cells. *Mol Carcinog*. 2015;54:1529–40.
25. Buick RN, Pullano R, Trent JM. Comparative properties of five human ovarian adenocarcinoma cell lines. *Cancer Res*. 1985;45:3668–76.
26. Cailleau R, Young R, Olivé M, Reeves WJ. Breast tumor cell lines from pleural effusions. *J Natl Cancer Inst*. 1974;53:661–74.
27. Harrell JC, Dye WW, Allred DC, Jedlicka P, Spoelstra NS, Sartorius CA, et al. Estrogen receptor positive breast cancer metastasis: altered hormonal

- sensitivity and tumor aggressiveness in lymphatic vessels and lymph nodes. *Cancer Res.* 2006;66:9308–15.
28. Pinto MP, Badtke MM, Dudevoir ML, Chuck Harrell J, Jacobsen BM, Horwitz KB. Vascular endothelial growth factor secreted by activated stroma enhances angiogenesis and hormone-independent growth of Estrogen receptor-positive breast cancer. *Cancer Res.* 2010.
 29. Ibáñez CC, Garrido SM, Medina L, Kato S, Bravo ML, González P, et al. In vitro cell response to chemotherapeutic agents, to personalize ovarian cancer treatment. Report of two cases. *Rev Med Chil.* 2013;141:669–73.
 30. Erices R, Bravo ML, Gonzalez P, Oliva B, Racordon D, Garrido M et al. Metformin, at concentrations corresponding to the treatment of diabetes, potentiates the cytotoxic effects of carboplatin in cultures of ovarian cancer cells. *Reprod Sci [Internet].* 2013;20:1433–46. Available from: <http://www.ncbi.nlm.nih.gov/pubmed/23653391>
 31. Vilos C, Morales FA, Solar PA, Herrera NS, Gonzalez-Nilo FD, Aguayo DA, et al. Paclitaxel-PHBV nanoparticles and their toxicity to endometrial and primary ovarian cancer cells. *Biomaterials.* 2013;34:4098–108.
 32. Quezada M, Diaz J, Henriquez S, Bravo ML, Aranda E, Oliva B, et al. 2-methoxyestradiol inhibits progesterone-dependent tissue factor expression and activity in breast cancer cells. *Horm Cancer.* 2010;1:117–26.
 33. Kato S, Smalley S, Sadarangani A, Chen-Liu K, Oliva B, Brañes J, et al. Lipophilic but not hydrophilic Statins selectively induce cell death in gynaecological cancers expressing high levels of HMGCoA reductase. *J Cell Mol Med.* 2010;14:1180–93.
 34. Kato S, Pinto M, Carvajal A, Espinoza N, Monso C, Sadarangani A, et al. Progesterone increases tissue factor gene expression, procoagulant activity, and invasion in the breast cancer cell line ZR-75-1. *J Clin Endocrinol Metab.* 2005;90:1181–8.
 35. Kato S, Pinto M, Carvajal A, Espinoza N, Monsó C, Bravo L, et al. Tissue factor is regulated by epidermal growth factor in normal and malignant human endometrial epithelial cells. *Thromb Haemost.* 2005. <https://doi.org/10.1160/TH05-01-0066>.
 36. Borza CM, Su Y, Chen X, Yu L, Mont S, Chetyrkin S, et al. Inhibition of integrin α2β1 ameliorates glomerular injury. *J Am Soc Nephrol.* 2012;23:1027–38.
 37. Miller MW, Basra S, Kulp DW, Billings PC, Choi S, Beavers MP, et al. Small-molecule inhibitors of integrin α 2 β 1 that prevent pathological thrombus formation via an allosteric mechanism. *Proc Natl Acad Sci U S A.* 2009;106:719–24.
 38. Arimori T, Miyazaki N, Miura E, Takizawa M, Taniguchi Y, Cabanás C, et al. Structural mechanism of laminin recognition by integrin. *Nat Commun [Internet].* 2021;12:1–13. Available from: <https://doi.org/10.1038/s41467-021-24184-8>
 39. Yokosaki Y, Palmer EL, Prieto AL, Crossin KL, Bourdon MA, Pytela R, et al. The integrin α9β1 mediates cell attachment to a non-RGD site in the third fibronectin type III repeat of Tenascin. *J Biol Chem.* 1994;269:26691–6.
 40. Illera MJ, Cullinan E, Gui Y, Yuan L, Beyler SA, Lessey BA. Blockade of the α(v)β3 integrin adversely affects implantation in the mouse. *Biol Reprod.* 2000;62:1285–90.
 41. Edgar R, Domrachev M, Lash AE. Gene expression omnibus: NCBI gene expression and hybridization array data repository. *Nucleic Acids Res.* 2002;30:207–10.
 42. Lezcano C, Kleffel S, Lee N, Larson AR, Zhan Q, Rosario A, Do et al. Merkel cell carcinoma expresses vasculogenic mimicry: Demonstration in patients and experimental manipulation in xenografts. *Lab Investig [Internet].* 2014;94:1092–102. Available from: <https://doi.org/10.1038/labinvest.2014.99>
 43. Larson AR, Lee CW, Lezcano C, Zhan Q, Huang J, Fischer AH, et al. Melanoma spheroid formation involves laminin-associated vasculogenic mimicry. *Am J Pathol.* 2014;184:71–8. <https://doi.org/10.1016/j.ajpath.2013.09.020>
 44. Saha D, Mitra D, Alam N, Sen S, Mitra Mustafi S, Mandal S, et al. Orchestrated expression of vasculogenic mimicry and laminin-5γ2 is an independent prognostic marker in oral squamous cell carcinoma. *Int J Exp Pathol.* 2022;103:54–64.
 45. Saha D, Mitra D, Alam N, Sen S, Mustafi SM, Majumder PK, et al. Lupeol and Paclitaxel cooperate in hindering hypoxia induced vasculogenic mimicry via suppression of HIF-1α-EphA2-Laminin-5γ2 network in human oral cancer. *J Cell Commun Signal.* 2023;17:591–608. <https://doi.org/10.1007/s12079-022-0693-z>
 46. Hess AR, Hendrix MJC. Focal adhesion kinase signaling and the aggressive melanoma phenotype. *Cell Cycle.* 2006;5:478–80.
 47. Kawahara R, Niwa Y, Simizu S. Integrin β1 is an essential factor in vasculogenic mimicry of human cancer cells. *Cancer Sci.* 2018;109:2490–6.
 48. Wang B, Yu Rze, Zhang X, yang, Ren Y, Zhen Y, wei, Han L. Polo-like kinase 4 accelerates glioma malignant progression and vasculogenic mimicry by phosphorylating EphA2. *Cancer Lett [Internet].* 2025;611:217397. Available from: <https://doi.org/10.1016/j.canlet.2024.217397>
 49. Yeo C, Lee HJ, Lee EO. Serum promotes vasculogenic mimicry through the EphA2/VE-cadherin/AKT pathway in PC-3 human prostate cancer cells. *Life Sci.* 2019;221:267–73. <https://doi.org/10.1016/j.lfs.2019.02.043>
 50. Shanthi E, Krishna MH, Arunesh GM, Venkateswara Reddy K, Sooriya Kumar J, Viswanadhan VN. Focal adhesion kinase inhibitors in the treatment of metastatic cancer: a patent review. *Expert Opin Ther Pat.* 2014;24:1077–100.
 51. Lim Y, Park H, Jeon J, Han I, Kim J, Jho EH, et al. Focal adhesion kinase is negatively regulated by phosphorylation at tyrosine 407. *J Biol Chem.* 2007;282:10398–404. <https://doi.org/10.1074/jbc.M609302200>
 52. Hunger-Glaser I, Fan RS, Perez-Salazar E, Rozengurt E. PDGF and FGF induce focal adhesion kinase (FAK) phosphorylation at Ser-910: dissociation from Tyr-397 phosphorylation and requirement for ERK activation. *J Cell Physiol.* 2004;200:213–22.
 53. Le Bœuf F, Houle F, Sussman M, Huot J. Phosphorylation of focal adhesion kinase (FAK) on Ser732 is induced by Rho-dependent kinase and is essential for proline-rich tyrosine kinase-2-mediated phosphorylation of FAK on Tyr407 in response to vascular endothelial growth factor. *Mol Biol Cell.* 2006. <https://doi.org/10.1091/mbc.e05-12-1158>
 54. Jiang W, Cai F, Xu H, Lu Y, Chen J, Liu J, et al. Extracellular signal regulated kinase 5 promotes cell migration, invasion and lung metastasis in a FAK-dependent manner. *Protein Cell.* 2020;11:825–45. <https://doi.org/10.1007/s138-020-00701-1>
 55. Cicenas J. The potential role of Akt phosphorylation in human cancers. *Int J Biol Markers.* 2008;23:1–9.
 56. Casamayor A, Morrice NA, Alessi DR. Phosphorylation of Ser-241 is essential for the activity of 3-phosphoinositide-dependent protein kinase-1: identification of five sites of phosphorylation in vivo. *Biochem J.* 1999;342:287–92.
 57. Yang Z, Xie C, Xu W, Liu G, Cao X, Li W, et al. Phosphorylation and inactivation of PTEN at residues Ser380/Thr382/383 induced by *Helicobacter pylori* promotes gastric epithelial cell survival through PI3K/Akt pathway. *Oncotarget.* 2015;6:31916–26.
 58. Liu H, Wang H, Chen D, Gu C, Huang J, Mi K. Endoplasmic reticulum stress inhibits 3D matrigel-induced vasculogenic mimicry of breast cancer cells via TGF-β1/Smad2/3 and β-catenin signaling. *FEBS Open Bio.* 2021;11:2607–18.
 59. Zhang J, Liu K, Peng P, Li S, Ye Z, Su Y, et al. Upregulation of nectin-4 is associated with ITGB1 and vasculogenic mimicry and May serve as a predictor of poor prognosis in colorectal cancer. *Oncol Lett.* 2019;18:1163–70.
 60. Weston CA, Anova L, Rialas C, Prives JM, Weeks BS. Laminin-1 activates Cdc42 in the mechanism of laminin-1-mediated neurite outgrowth. *Exp Cell Res.* 2000;260:374–8.
 61. Resendiz-Hernández M, García-Hernández AP, Silva-Cázares MB, Coronado-Uribe R, Hernández-de la Cruz ON, Arriaga-Pizano LA et al. MicroRNA-204 regulates angiogenesis and vasculogenic mimicry in CD44+/CD24- breast cancer Stem-like cells. *Non-coding RNA.* 2024;10.
 62. Contreras-Sanzón E, Carlos-Reyes Á, Sierra-Martínez M, Acosta-Altamirano G, Luna-Rivero C, Núñez-Corona D, et al. Metastatic breast tumors downregulate miR-145 regulating the hypoxia-induced vasculogenic mimicry. *Transl Oncol.* 2023. <https://doi.org/10.1016/j.tranon.2023.101680>
 63. de Visser KE, Joyce JA. The evolving tumor microenvironment: from cancer initiation to metastatic outgrowth. *Cancer Cell.* 2023;41:374–403. <https://doi.org/10.1016/j.ccr.2023.02.016>
 64. Deasy SK, Erez N. A glitch in the matrix: organ-specific matrisomes in metastatic niches. *Trends Cell Biol.* 2022;32:110–23. <https://doi.org/10.1016/j.tcb.2021.08.001>
 65. Kleinman HK, Martin GR, Matrigel. Basement membrane matrix with biological activity. *Semin Cancer Biol.* 2005;15:378–86.
 66. Benton G, Arnaoutova I, George J, Kleinman HK, Koblinski J, Matrigel. From discovery and ECM mimicry to assays and models for cancer research. *Adv Drug Deliv Rev [Internet].* 2014;79:3–18. Available from: <https://doi.org/10.1016/j.addr.2014.06.005>
 67. Liu S, Kang M, Ren Y, Zhang Y, Ba Y, Deng J, et al. The interaction between vasculogenic mimicry and the immune system: mechanistic insights and dual exploration in cancer therapy. *Cell Prolif.* 2025. <https://doi.org/10.1111/cpr.13814>

68. Ge SX, Son EW, Yao R, iDEP. An integrated web application for differential expression and pathway analysis of RNA-seq data. BMC Bioinformatics. 2018;19:1–24.

Publisher's Note

Springer Nature remains neutral with regard to jurisdictional claims in published maps and institutional affiliations.